Supplementary Figure S1

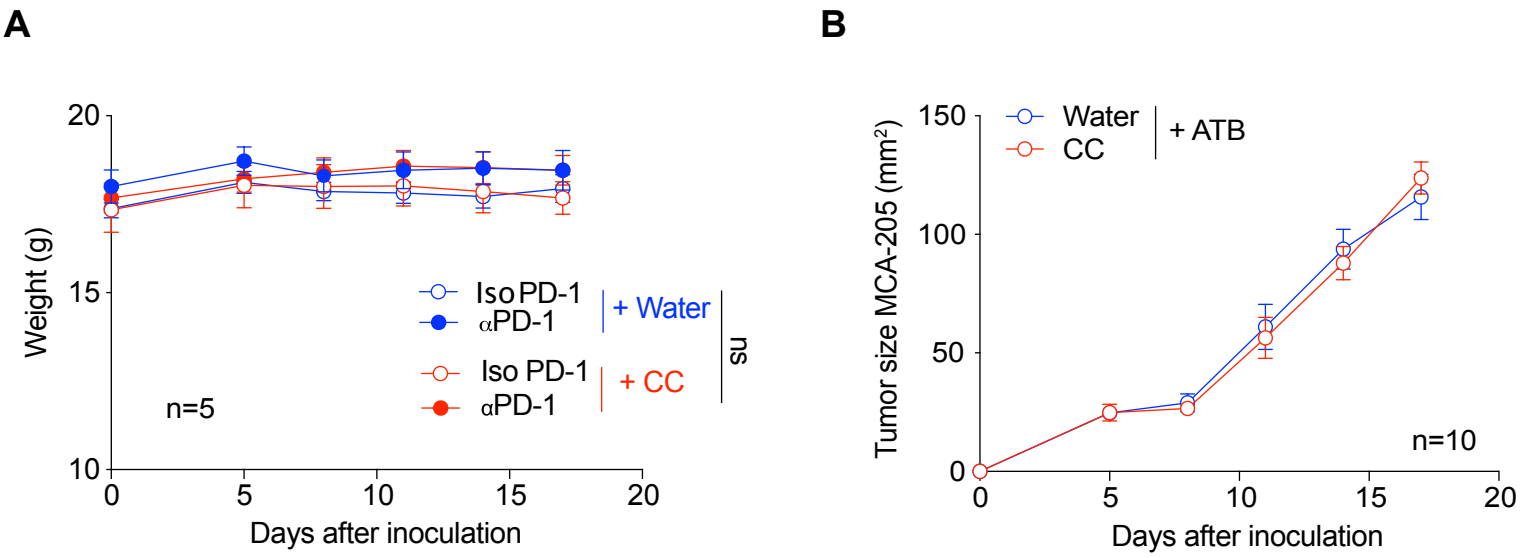

Supplementary Figure S1. CC did not modify the murine weight and its antitumor activity requires an intact microbiome. **A.** Representative weight kinetics in SPF C57Bl/6 mice inoculated with MCA-205 after sequential injections of anti-PD-1 mAb (αPD-1) or isotype control mAb (IsoPD-1) and daily oral gavage with water or CC. **B.** MCA-205 tumor growth kinetics in mice treated with broad spectrum antibiotics (ATB) with daily oral gavage with water or CC (n=10 mice/group). Means ± SEM are represented. ns: non-significant.

Supplementary Figure S2

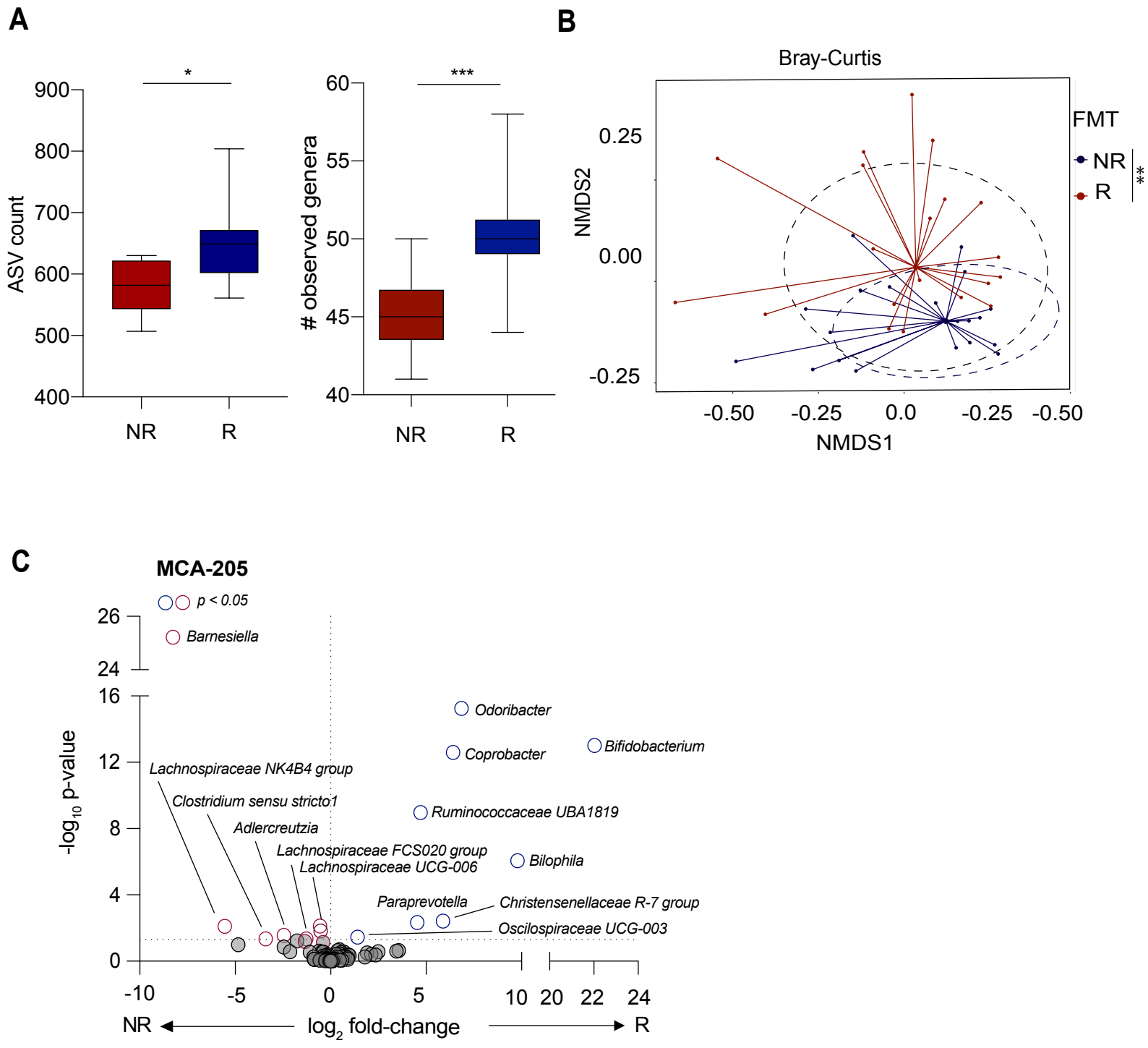

Supplementary Figure S2. Differences in microbiome composition post-FMT between R and NR patients. **A.** Amplicon sequence variant (ASV) count (left) and number of observed species (right) representation for the alpha diversity of NR and R at baseline (before CC gavage) after 14 days of engraftment in MCA-205-bearing SPF mice that were treated with ATB before receiving FMT from NSCLC patients (NR1, R1), transplanted in 10 animals for each patient. **B.** Bray-Curtis representation of the beta diversity of the 16S rRNA sequencing after 2 weeks of engraftment of NR and R FMT at the genus level. **C.** Volcano plot representation of differential abundance analysis (unadjusted p-value) results after 16S rRNA sequencing of feces from mice that received NR or R FMT prior to initiation of CC +/- aPD-1 (D+5). *p < 0.05, **p < 0.01 and ***p < 0.001.

Supplementary Figure S3

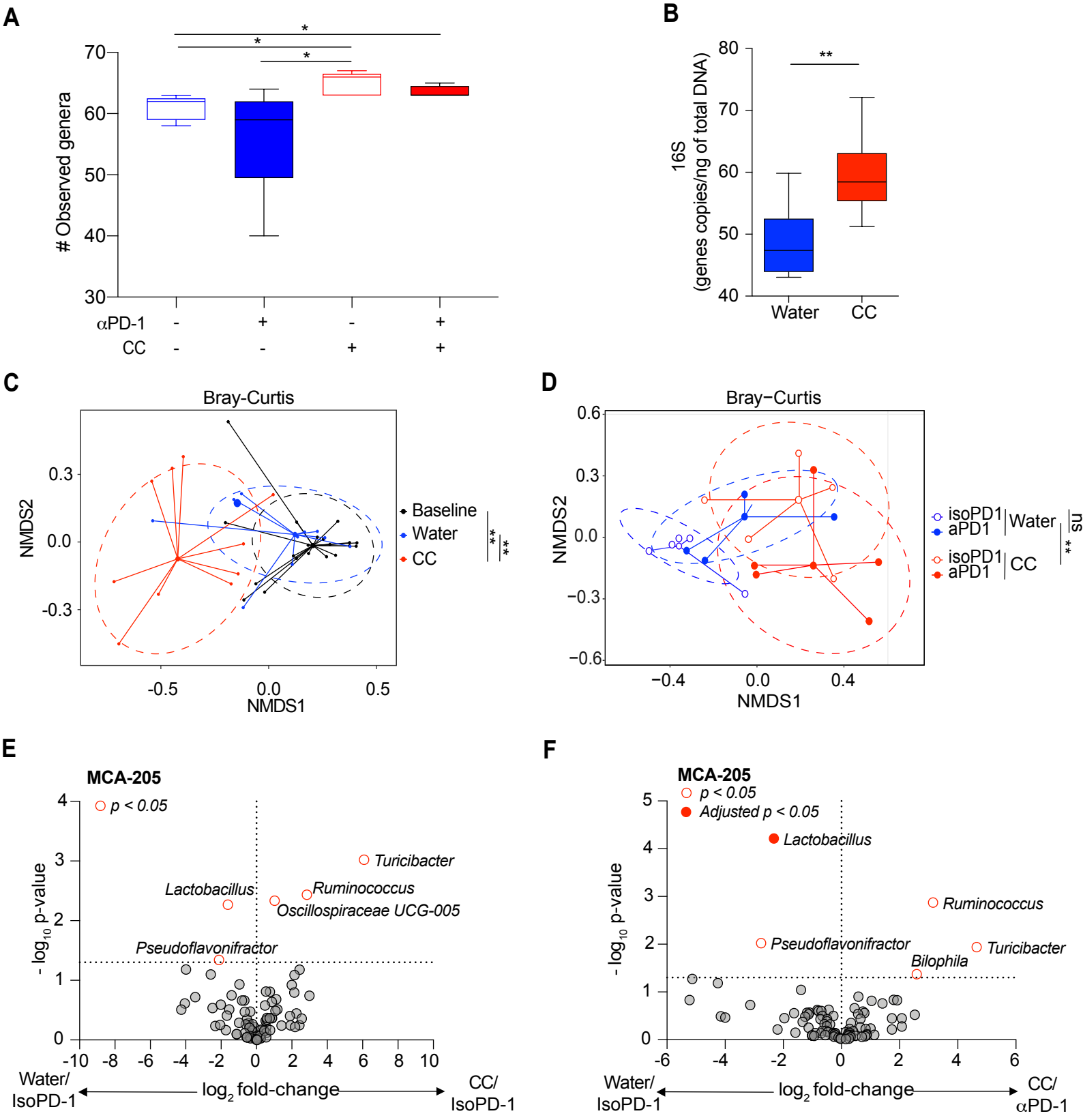

Supplementary Figure S3. Shift in the gut microbiota composition in MCA-205 tumor model post-CC supplementation. A. 16S rRNA analysis of the fecal samples from mice from the four groups in the MCA-205 experiments, and representation of the alpha diversity measured by the observed genera in each group. **B.** Real-time PCR on DNA extracted from mouse feces after oral gavage of CC or water using specific primers for 16S rRNA detection in the MCA-205 model (n=10 mice/group). **C.** Beta diversity measured by Bray-Curtis index comparing baseline (pre-treatment) with CC (αPD-1 and IsoPD-1) or water (αPD-1 and IsoPD-1) groups. **D.** 16S rRNA microbiome profiling of samples from MCA-205 experiments and representation of beta diversity measured by Bray-Curtis index comparing all four groups. **E.** Volcano plot representation of differential abundance analysis in the water/IsoPD-1 vs. CC/IsoPD-1 groups and (F) water/IsoPD-1 vs. CC/αPD-1 groups in the MCA-205 tumor model. Bacteria enriched in each group are represented using adjusted p-value (fill shape symbol) and p-value (no fill shape symbol) (false discovery rate: 0.05). ns: non-significant, *p < 0.05, and **p < 0.01. NMDS: nonmetric multidimensional scaling.

Supplementary Figure 4

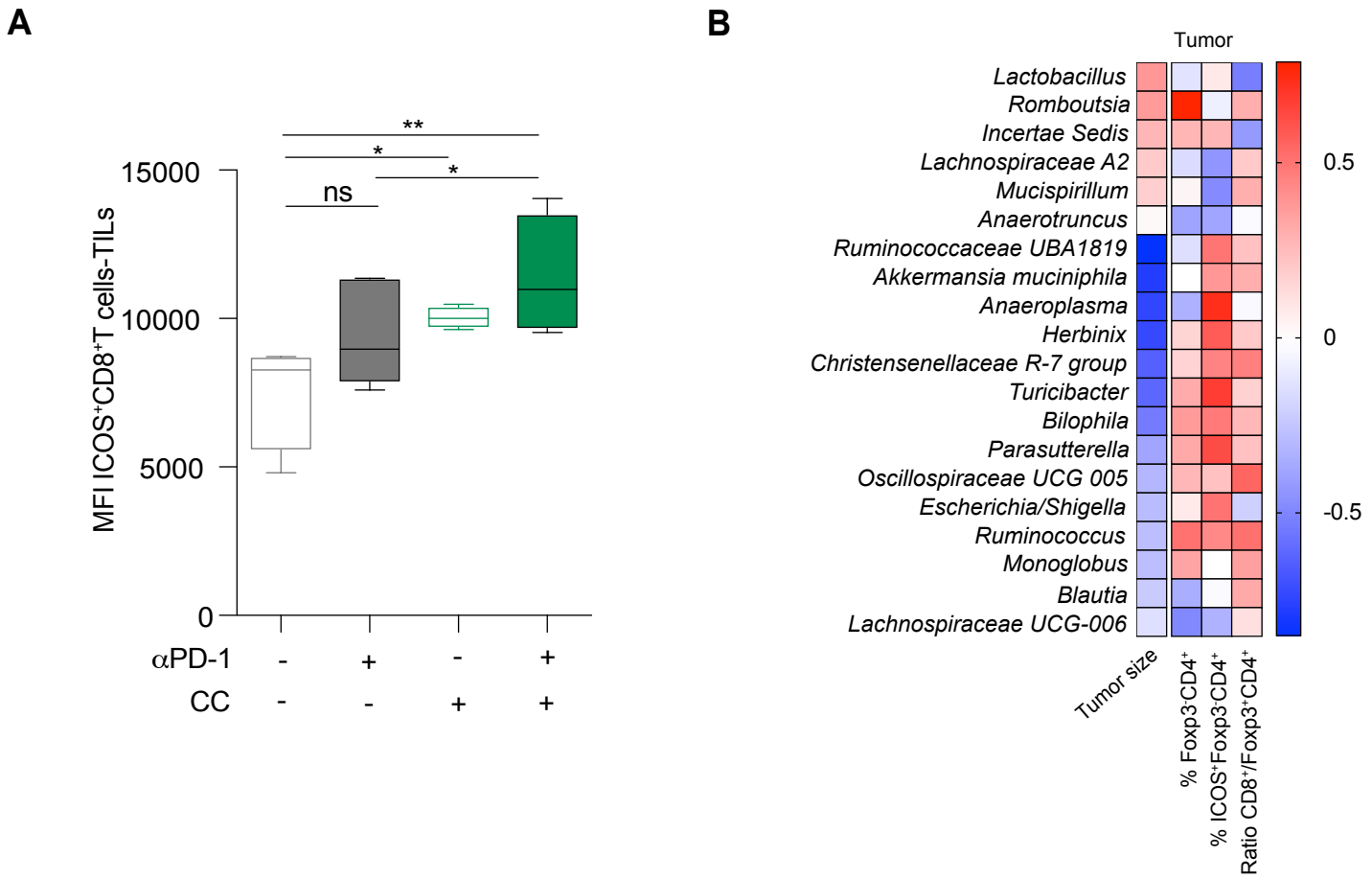

Supplementary Figure S4. Immune-potentiating effect of CC in the E0771 tumor model. A. Flow cytometry analysis of the mean fluorescence intensity (MFI) of $ICOS^+CD8^+$ T cells in E0771 TILs. **B.** Pairwise Spearman rank correlation heatmap between significantly different fecal taxa enriched in CC/αPD-1 vs. water/αPD-1 groups and frequency of indicated cell types by flow cytometry and matching tumor size in the E0771 tumor model. Unpaired t-tests were used in A. ns: non-significant, $*p < 0.05$ and $**p < 0.01$.

Supplementary Figure S5

A

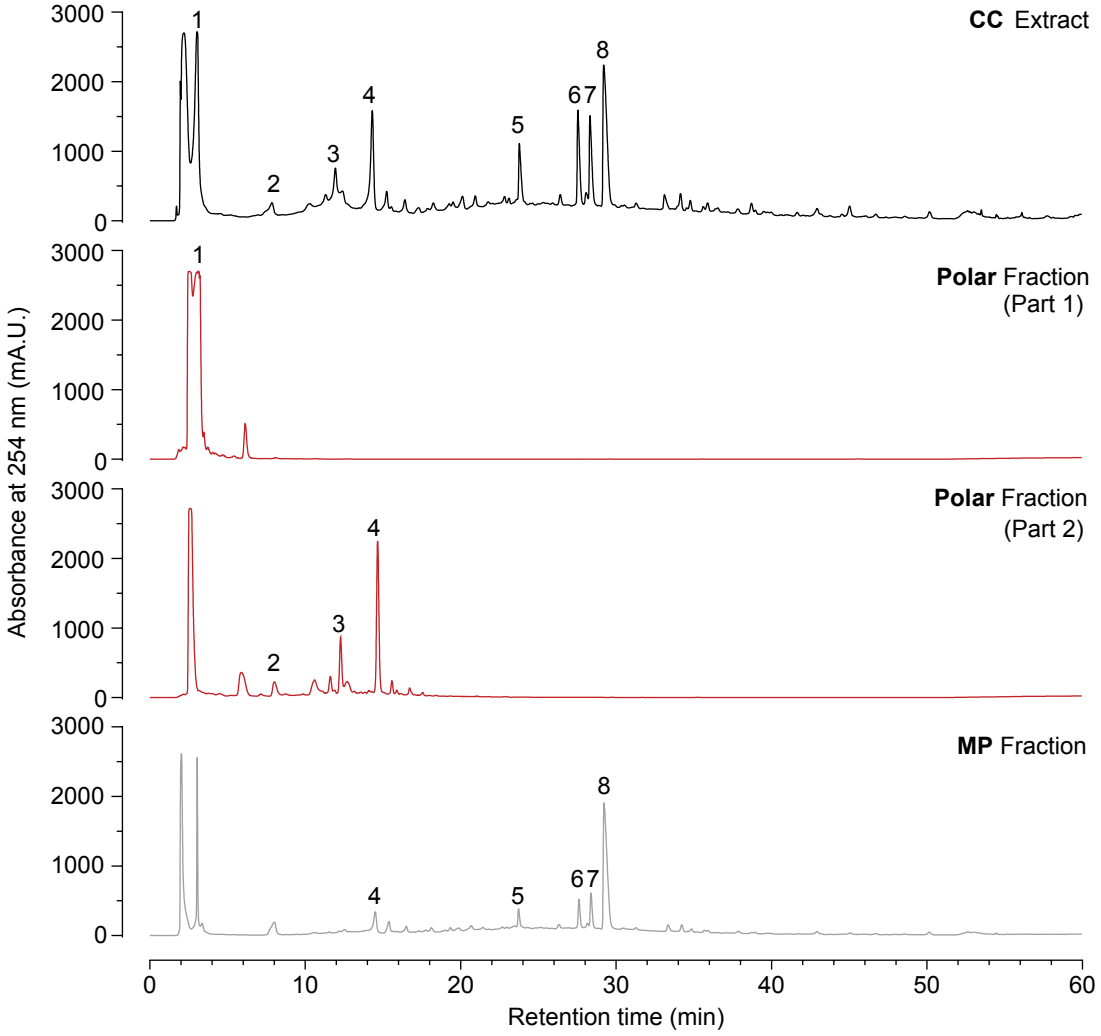

B

Number	Compound	Monoisotopic mass (g/mol)	$[M-H]^-$ found (m/z)
1	L-ascorbic acid	176.03	175.2
2	gallic acid	170.02	169.1
3	vescalagin	934.07	933.1
4	castalagin	934.07	933.1
5	ellagic acid hexoside	464.06	463.0
6	ellagic acid pentoside	434.05	433.2
7	ellagic acid hexoside	464.06	463.2
8	ellagic acid	302.01	301.1

Supplementary Figure S5. HPLC fractionation and LC-MS analysis of CC extract. A. Aligned chromatograms (λ = 254 nm) of isolated fractions from CC. Peak numbering is shown in (B). Both parts of the polar fraction (P) were isolated using solid-phase extraction, then combined. The medium polarity (MP) fraction was isolated from CC by extracting twice in water, then twice in 50% methanol. The contents of the 50% methanol extracts were used as the MP fraction. The non-polar (NP) fraction was isolated by preparative HPLC on the CC extract. Minutes 30-60 were collected. The insoluble fraction (INS) was isolated from CC by extracting twice in water, twice in 50% MeOH, and twice in 90% MeOH. The CC powder remaining after extraction gave rise to the INS raction. **B.** LC-MS analysis of major peaks present in the CC extract.

Supplementary Figure S6

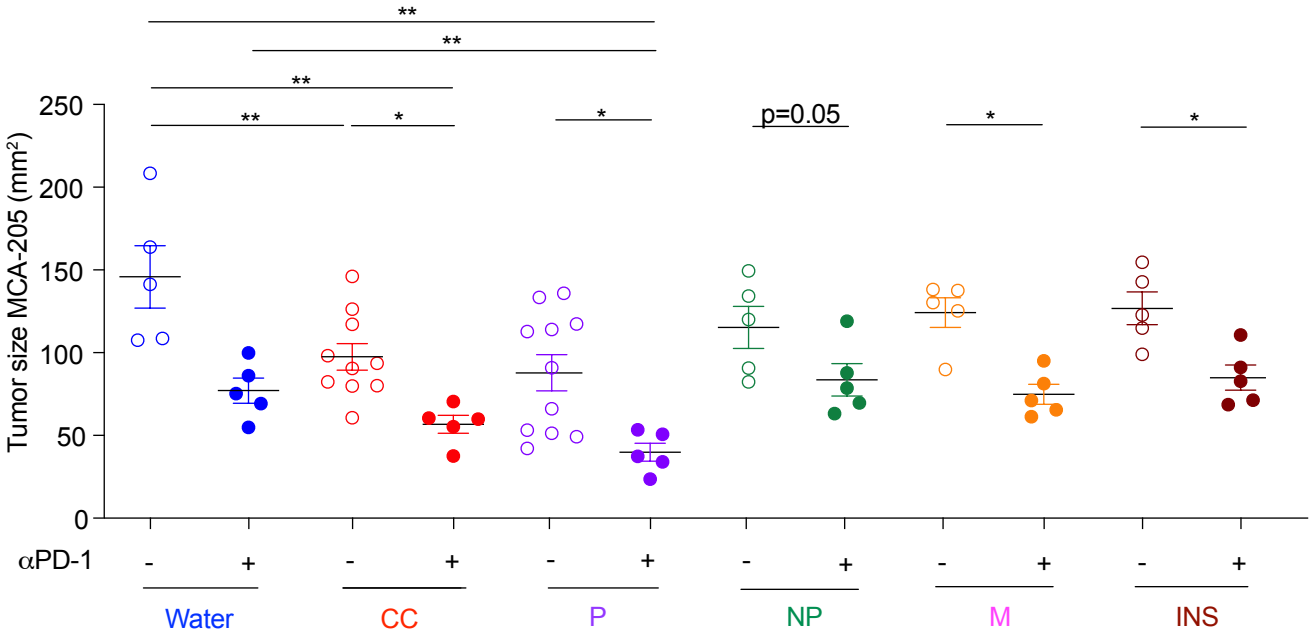

Supplementary Figure S6. Testing of different CC fractions in MCA-205 tumor model. Mean ± SEM of tumor sizes at sacrifice of MCA-205-bearing SPF mice after αPD-1 or IsoPD-1 treatment and daily oral gavage with water, CC or the four fractions isolated from CC based on their polarity (each circle represents one animal). Unpaired t-tests were used. *p < 0.05 and **p < 0.01.

Supplementary Figure S7

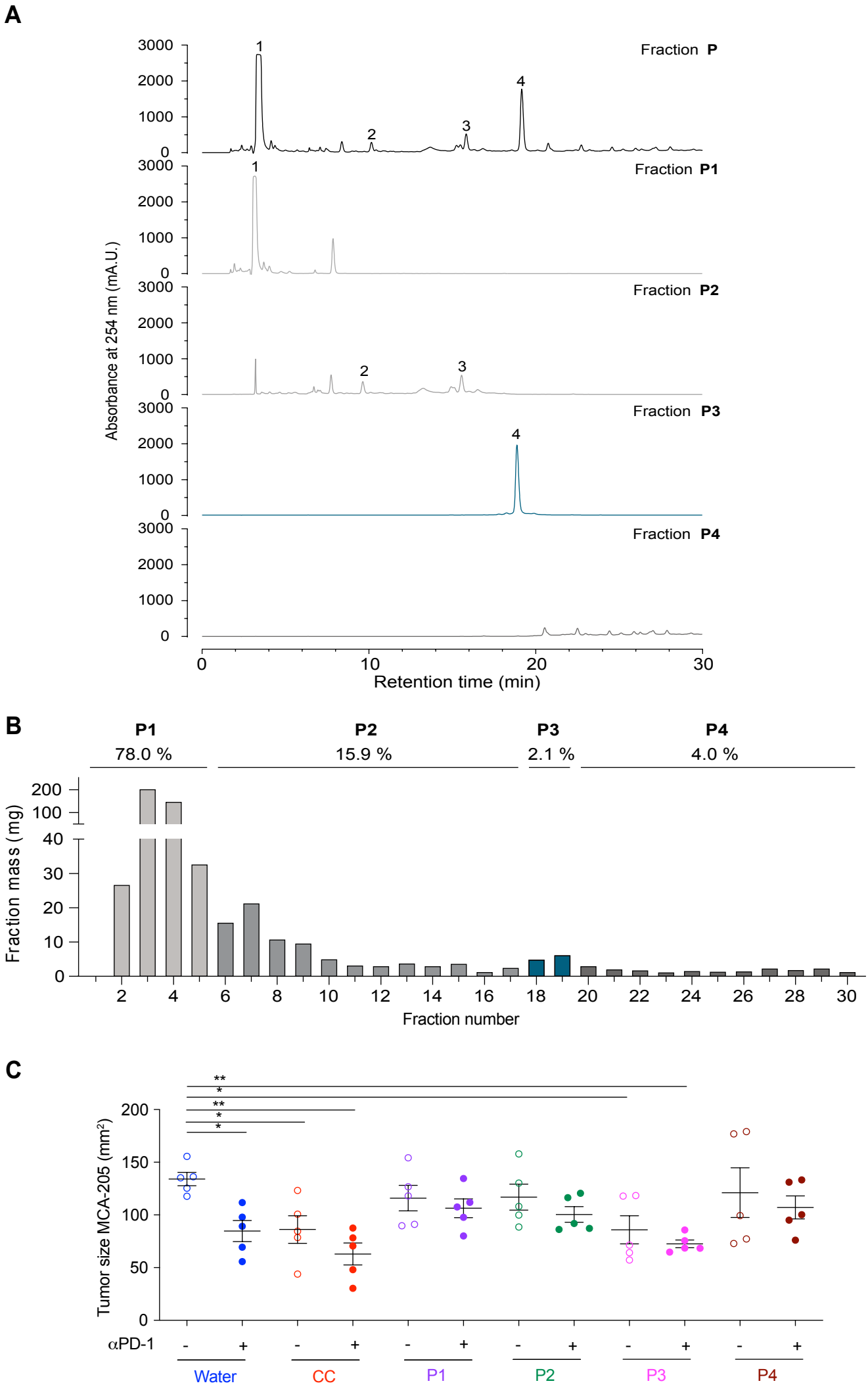

Supplementary Figure S7. HPLC fractionation of fraction P to produce sub-fractions P1-4 and their testing of different CC fractions in MCA-205 tumor model.. A. Aligned chromatograms (λ=254 nm) of isolated sub-fractions from fraction P. Fractions were collected every minute, then combined to produce sub-fractions P1-4. Peak numbering is the same as in Supplementary Figure S5B. **B.** Mass of fractions isolated from preparative HPLC runs (N=7) aligned with the chromatograms in (A). The isolated proportion of each combined fraction was used to calculate sub-fraction doses (as a proportion of the fraction P dose). **C.** Mean ± SEM of tumor sizes at sacrifice of MCA-205-bearing SPF mice after αPD-1 or IsoPD-1 treatment and daily oral gavage with water, CC or the four sub-fractions isolated from the polar fraction. Unpaired t-tests were used. *$p < 0.05$ and **$p < 0.01$.

Supplementary Figure S8

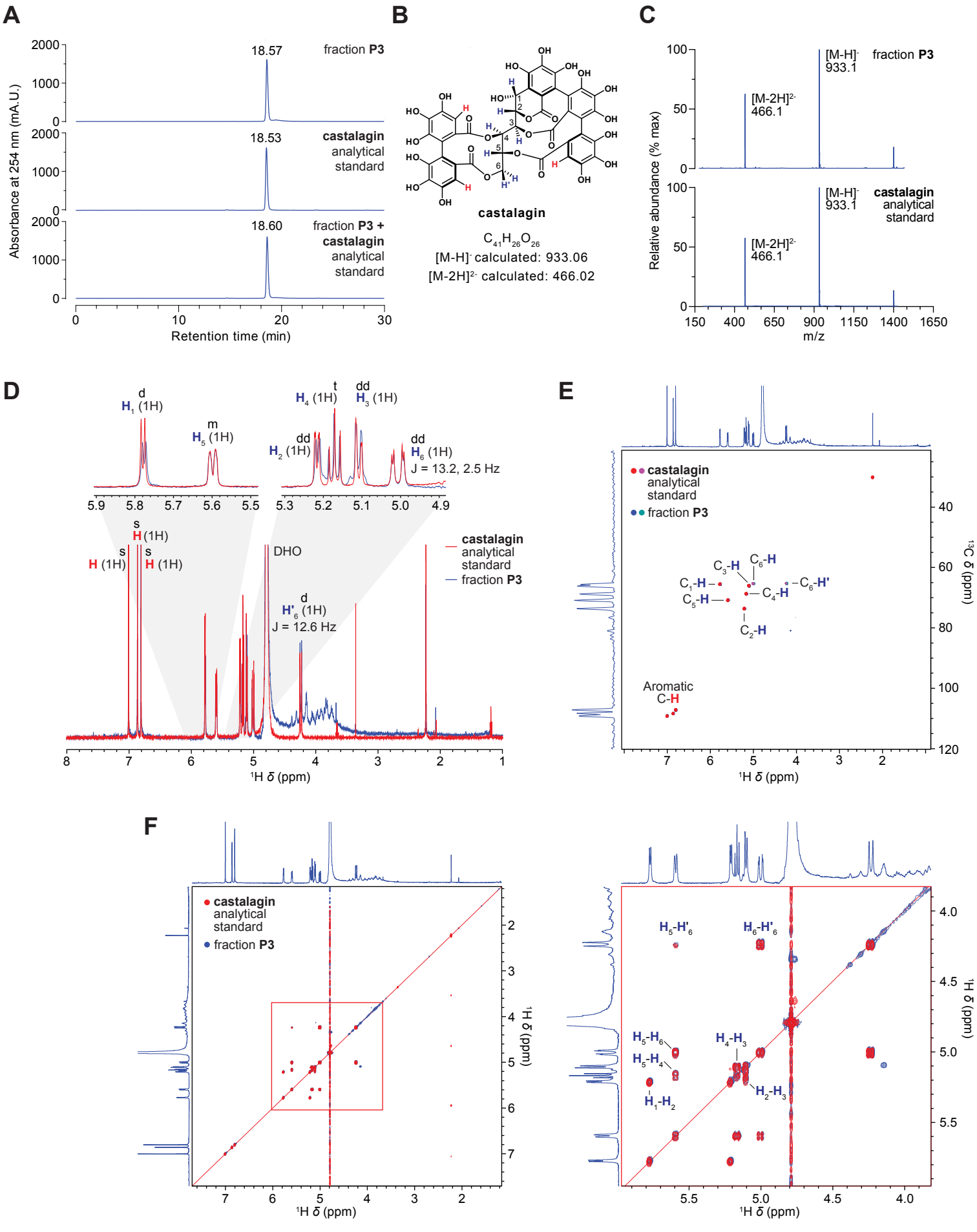

Supplementary Figure S8. Characterization of sub-fraction P3 by LC-MS and NMR spectroscopy. **A.** Aligned chromatograms (λ = 254 nm) from top to bottom: sub-fractionP3, a castalagin analytical standard, and an equimolar mixture of both. The injection volume for all samples was 10 µL. Retention times are noted above each peak. **B.** Chemical structure of castalagin with ^{1}H NMR-visible protons colored in blue (central carbon chain) or in red (aromatic groups). Calculated [M-H]- and $[M-2H]^{2-}$ ions for castalagin are shown below. **C.** Negative ESI-MS spectra of the main peak of sub-fraction P3 (top) and the castalagin analytical standard (bottom). **D.** Overlaid ^{1}H NMR spectrum (D2O, 500 MHz) of sub-fraction P3 (blue) and the castalagin analytical standard (red). The inset shows zoomed-in regions between 5.9-5.5 and 5.3-4.9 ppm for both samples. **E.** Overlaid HSQC NMR spectra of sub-fraction P3 (blue/turquoise) and the castalagin analytical standard (red/violet). The ^{1}H NMR and ^{13}C NMR (D_2O, 125 MHz) spectra of sub-fraction P3 are shown on the horizontal axis and the vertical axis, respectively. **F.** Overlaid COSY NMR spectra of sub-fraction P3 (blue) and the castalagin analytical standard (red). The 1H NMR spectrum of sub-fraction P3 is shown on both the horizontal and vertical axes. The red diagonal line denotes self-correlation of protons. Right panel shows zoomed-in area outlined by red square in the left panel.

Supplementary Figure S9

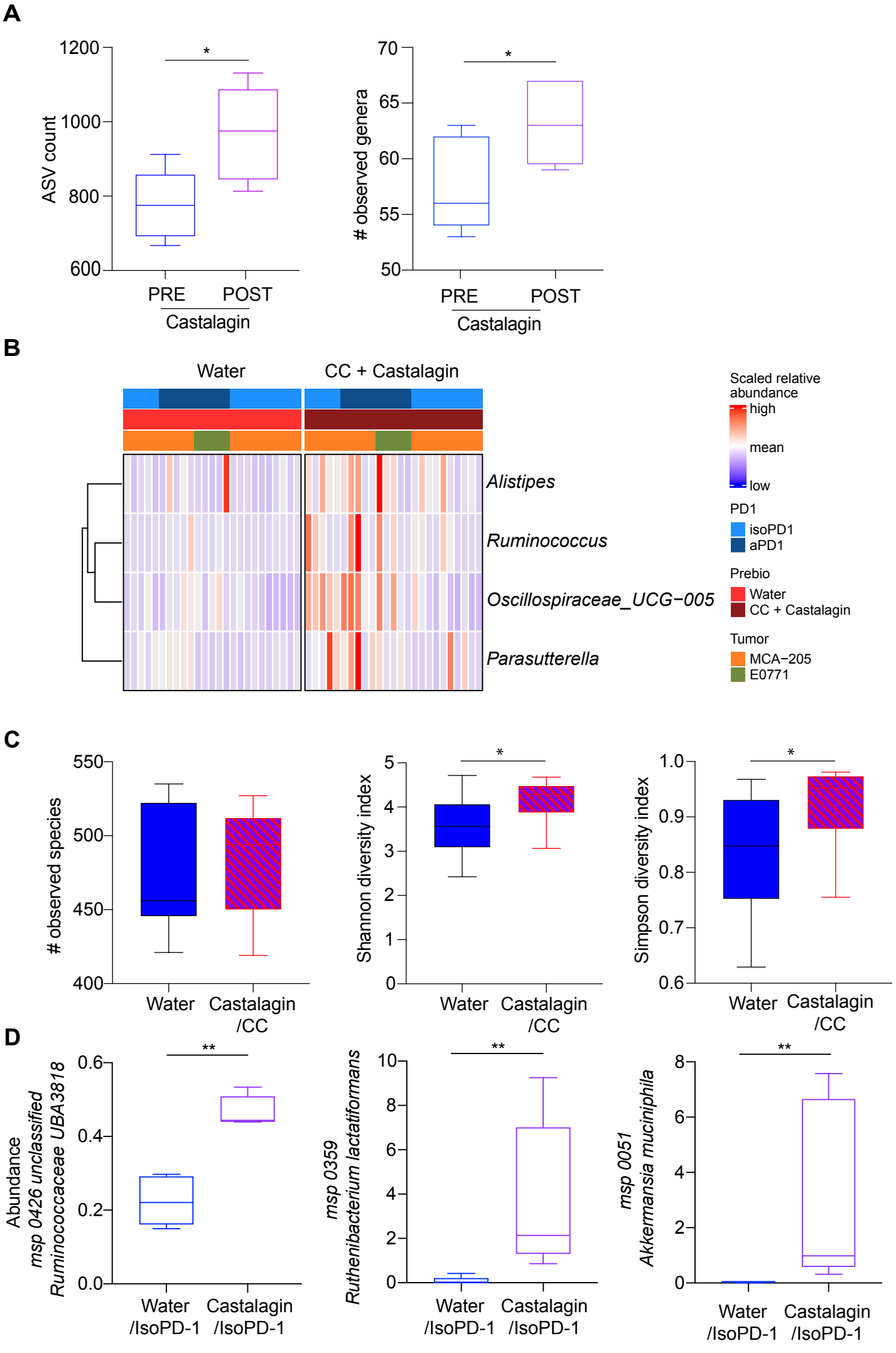

Supplementary Figure S9. Modification of the gut microbiome post-castalagin supplementation analyzed by 16S rRNA and metagenomics. A. Measurement of alpha diversity by16S rRNA sequencing representing ASV count and observed number of genera at baseline (PRE) and after castalagin gavage (POST) in the MCA-205 model. Unpaired t-tests were used and *p < 0.05. **B.** Heatmap combining all the 16S rRNA results from MCA-206 and E0771 mice treated with either CC or castalagin (αPD-1 and IsoPD-1) compared to water (αPD-1 and IsoPD-1) control. **C.** Measurement of alpha diversity by metagenomic sequencing representing observed species, Shannon, and Simpson indexes in water compared to CC/castalagin group (αPD-1 and IsoPD-1). Unpaired t-tests were used and *p < 0.05. **D.** Relative abundance representation from metagenomic sequencing comparing IsoPD-1/water vs. IsoPD-1/castalagin (n=5/group). Unpaired t-tests were used and **p < 0.01

Supplementary Figure S10

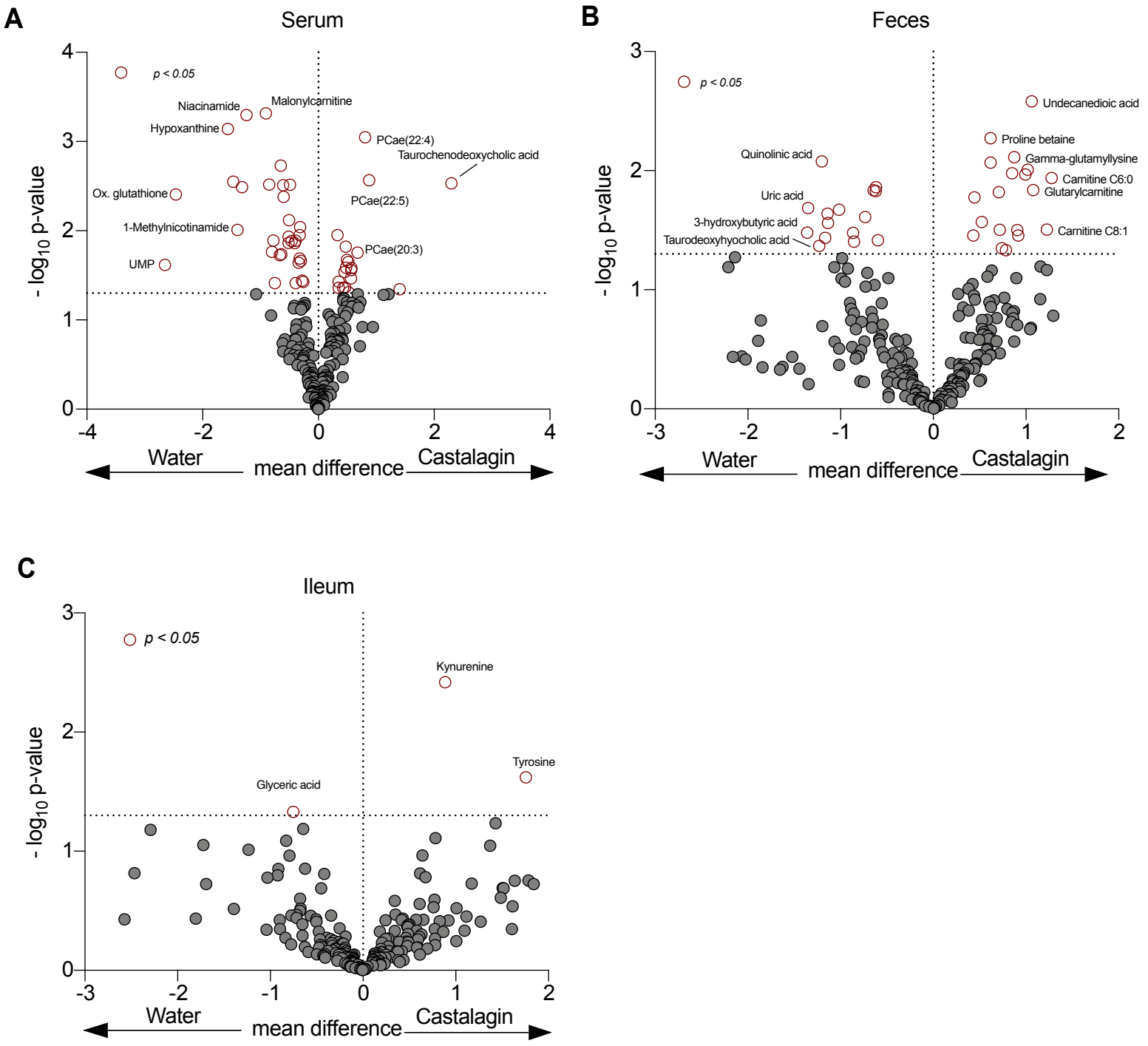

Supplementary Figure S10. Impact of castalagin on the gut microbiome production of metabolites. Differential metabolite identification in samples from **(A)** serum, **(B)** feces, and **(C)** ileum from mice receiving water or castalagin in the MCA-205 model (n=7mice/group). The horizontal dotted black line shows where p=0.05 with points above indicating metabolites with significantly different abundance (p<0.05).

Supplementary Figure S11

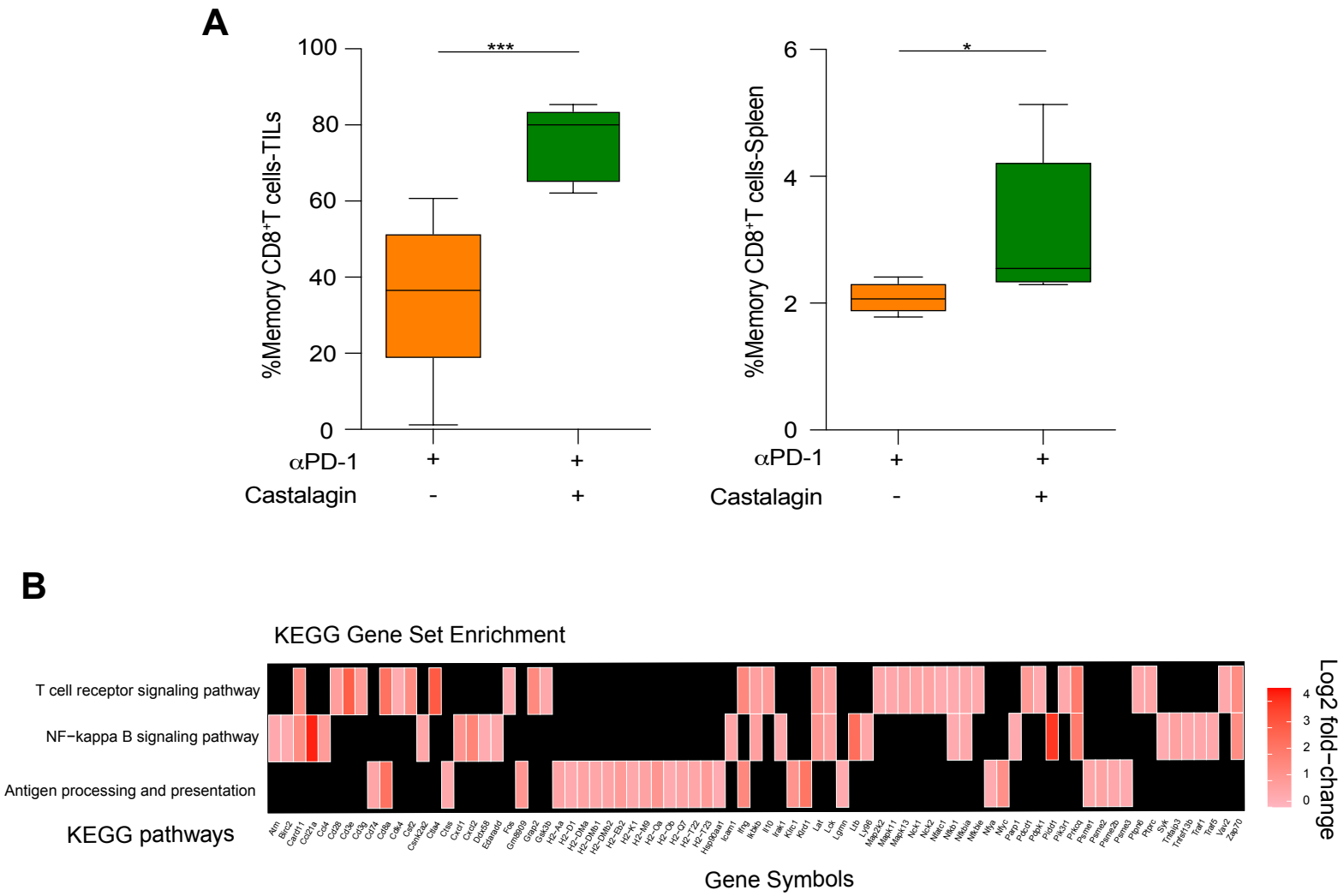

Supplementary Figure S11. Impact of castalagin on the immune response. A. Flow cytometry analysis (at sacrifice) of E0771 TILs (left panel) and splenocytes (right panel) depicting central memory (TCM) T cells among $CD8^+$ T cells (n=5/group). Unpaired t-tests were used, *$p < 0.05$ and ***$p < 0.001$. **B.** Heatmap plot of genes enriched in the different KEGG pathways between castalagin/IsoPD-1 vs. water/IsoPD-1 groups in the MCA-205 model. **C.** Comparison of the CIBERSORT estimated $CD8^+$ T cells between castalagin/IsoPD-1 vs. water/IsoPD-1 groups in the MCA-205 model.

Supplementary Figure S12

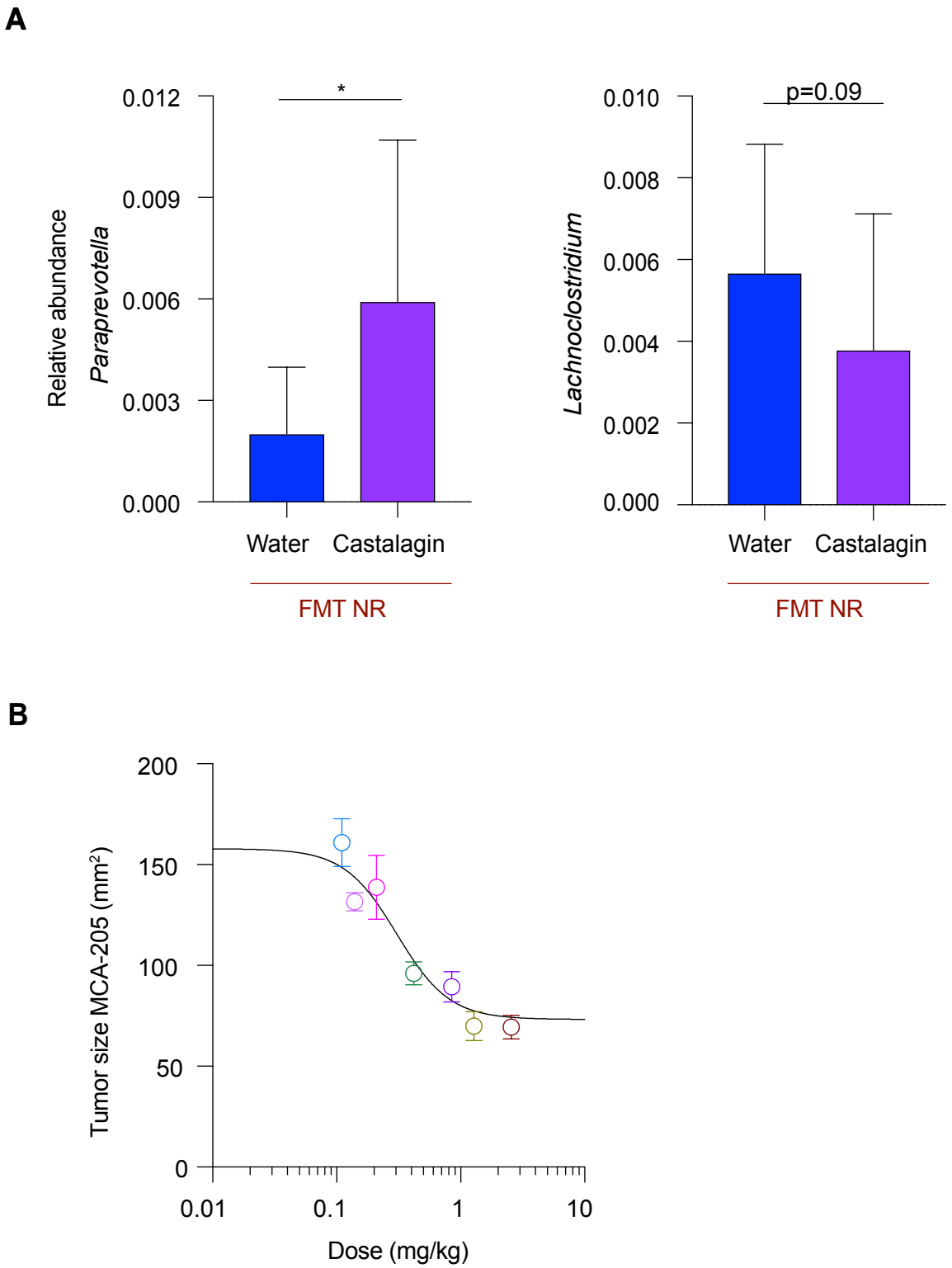

Supplementary Figure S12. Impact of castalagin on the gut microbiome composition. A. Relative abundance analysis of Paraprevotella and Lachnoclostridium between water and castalagin groups in the NR FMT experiments. Unpaired t-tests were used. **B.** Castalagin antitumor dose-response curve in MCA-205 tumor model. Means ± SEM are represented in all graphs. *p < 0.05.

Supplementary Figure S13

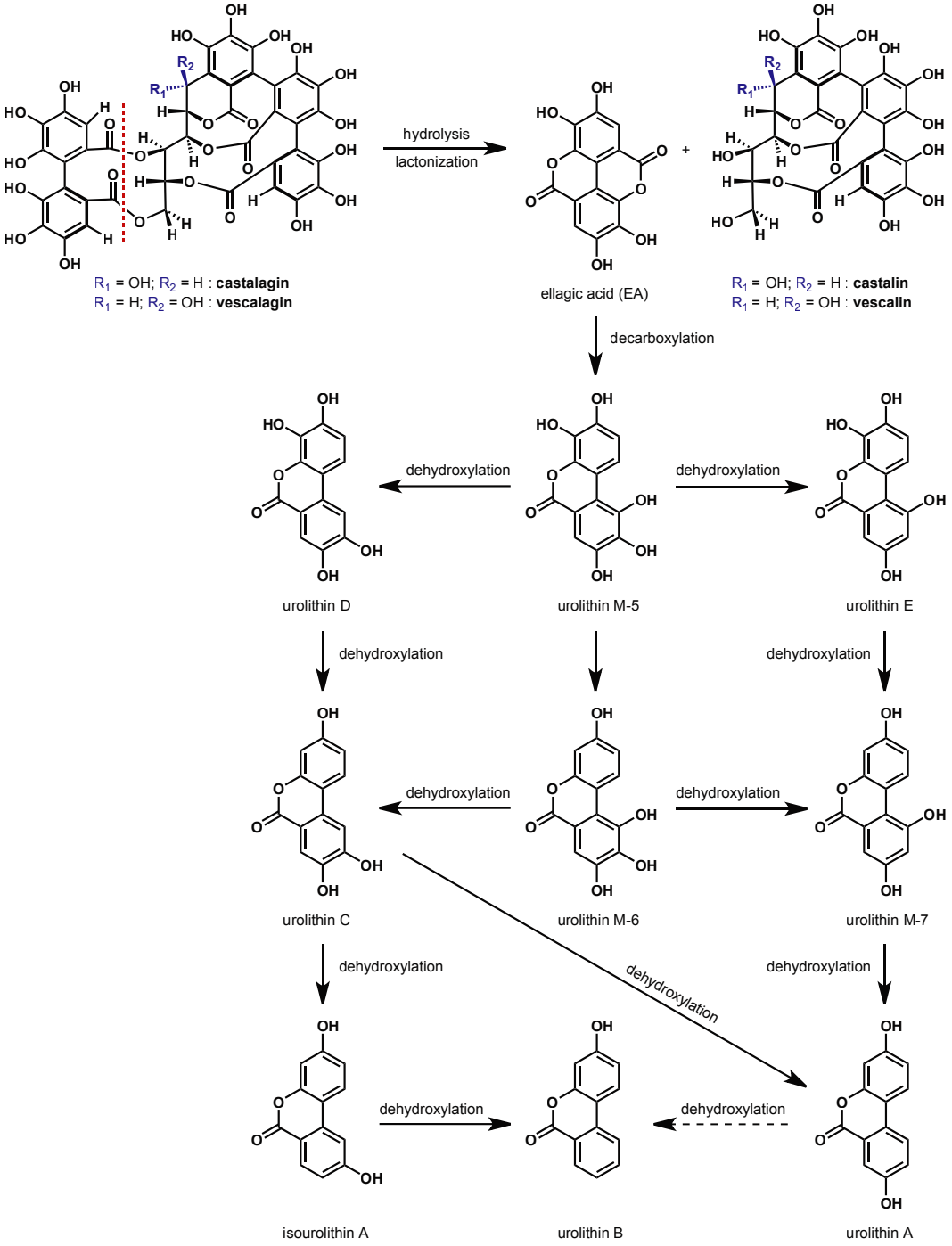

Supplementary Figure S13. Castalagin metabolism and downstream metabolites. Ellagitannin (castalagin and vescalagin) catabolic pathway by the gut microbiota. Castalagin and vescalagin are hydrolyzed to release ellagic acid and either castalin or vescalin. Ellagic acid is then converted to different urolithins through a decarboxylation reaction and a series of dehydroxylation reactions, some of which are known to be catalyzed by gut bacteria.

Supplementary Figure S14

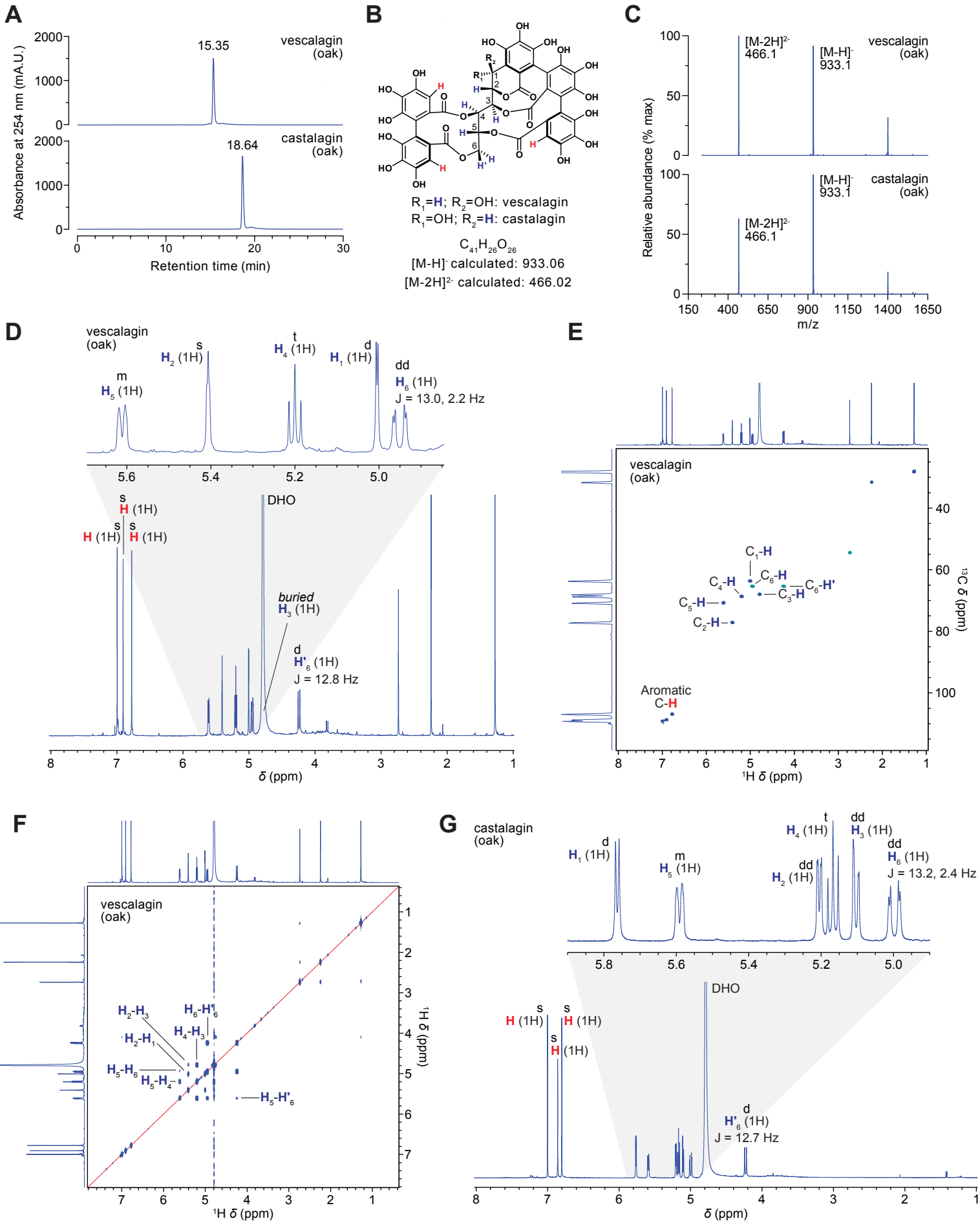

Supplementary Figure S14. Characterization of vescalagin and castalagin isolated from oak wood (*Quercus sp.*). A. Aligned chromatograms (λ = 254 nm) of vescalagin (top) and castalagin (bottom) isolated from oak. The injection volume for all samples was 10 µL. Retention times are noted above each peak. **B.** Chemical structure of the diastereomers vescalagin and castalagin with ^{1}H NMR-visible protons colored in blue (central carbon chain) or in red (aromatic groups). Calculated [M-H]- and $[M-2H]^{2-}$ ions for vescalagin and castalagin are shown below. **C.** Negative ESI-MS spectra of the main peak of vescalagin (top) and castalagin (bottom). **D.** ^{1}H NMR spectrum (D_2O, 500 MHz) of vescalagin. Inset shows zoomed-in regions between 5.70-4.85 ppm. **E.** HSQC NMR spectrum of vescalagin. The ^{1}H NMR and ^{13}C NMR (D_2O, 125 MHz) spectra of vescalagin are shown on the horizontal axis and the vertical axis, respectively. **F.** COSY NMR spectrum of vescalagin. The ^{1}H NMR spectrum of vescalagin is shown on both the horizontal and vertical axes. The red diagonal line denotes self-correlation of protons. **G.** ^{1}H NMR spectrum (D_2O, 500 MHz) of castalagin isolated from oak wood. Supplementary Figure S8D shows the ^{1}H NMR spectrum of the castalagin analytical standard for reference.

Supplementary Figure S15

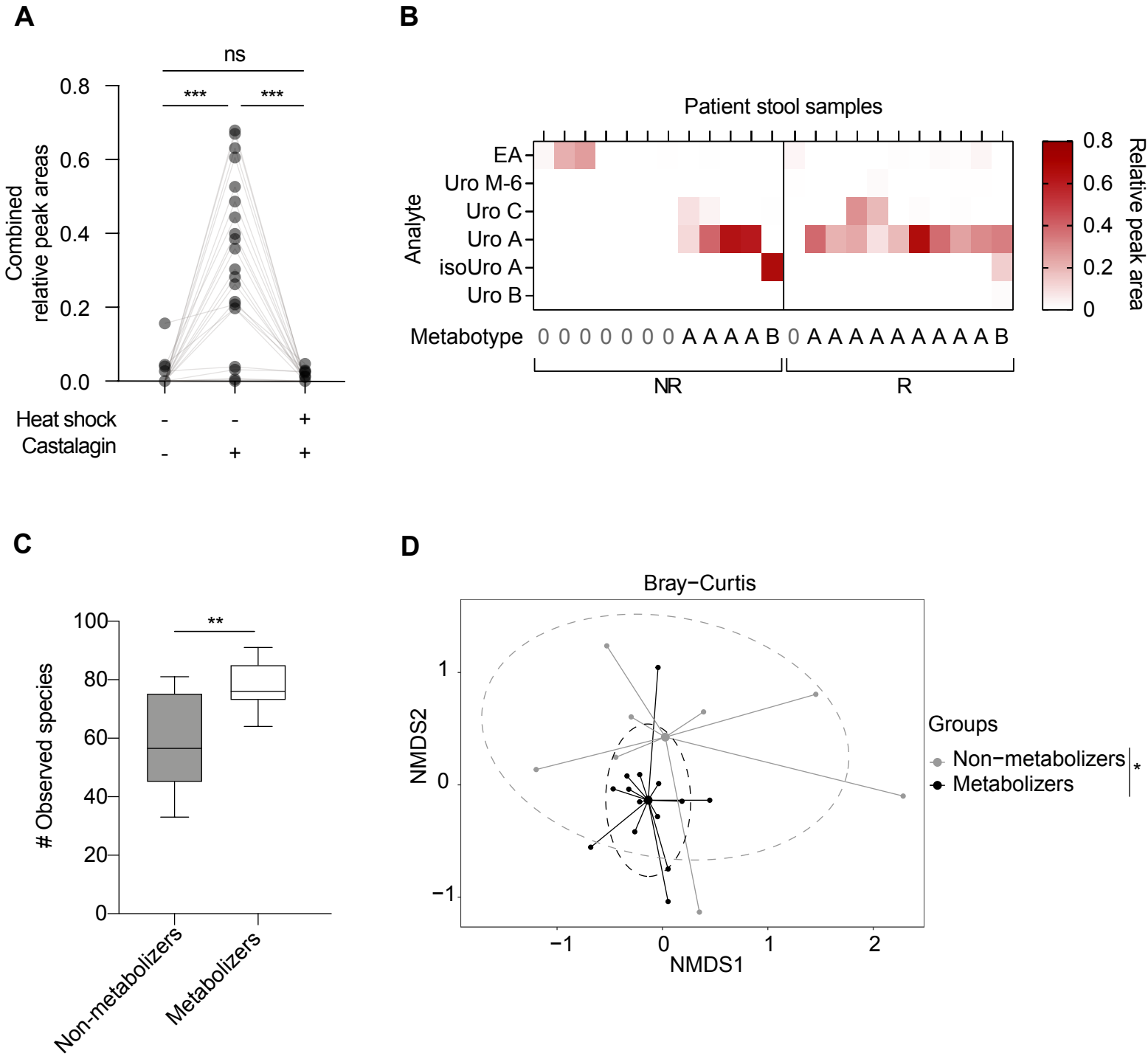

Supplementary Figure S15. Ex vivo castalagin metabolism by the gut microbiota of patients with NSCLC. A. Validation of ex vivo castalagin metabolism assay using fecal slurries from patients with NSCLC. Matched data points represent the same patient in different conditions. Combined relative peak areas (analyte/internal standard) for each analyte were used as a measure for overall metabolism. A repeated-measures one-way ANOVA with Tukey's multiple comparison test was used to compare all conditions to each other. ns: nonsignificant. ***$p < 0.001$. **B.** Relative peak area (analyte/internal standard) heatmap of ex vivo castalagin metabolism using fecal slurries from patients with NSCLC. Each column represents one patient. Metabolic phenotypes (metabotypes) are denoted for each patient below along with ICI response status. Patient urolithin metabolic phenotypes (metabotypes) were stratified according to the final urolithins produced in ex vivo metabolism assays: metabotype A (urolithin A exclusively), metabotype B (isourolithin A and/or urolithin B), and metabotype 0 (none of the final metabolites) (1). **C.** Metagenomics sequencing with representation of number of observed species in the 15 metabolizers and 8 non-metabolizers. **D.** Bray-Curtis representation of the beta diversity of the metagenomic analysis of the feces samples of metabolizers and non-metabolizers. *$p < 0.05$ and **$p < 0.01$.

Supplementary Figure S16

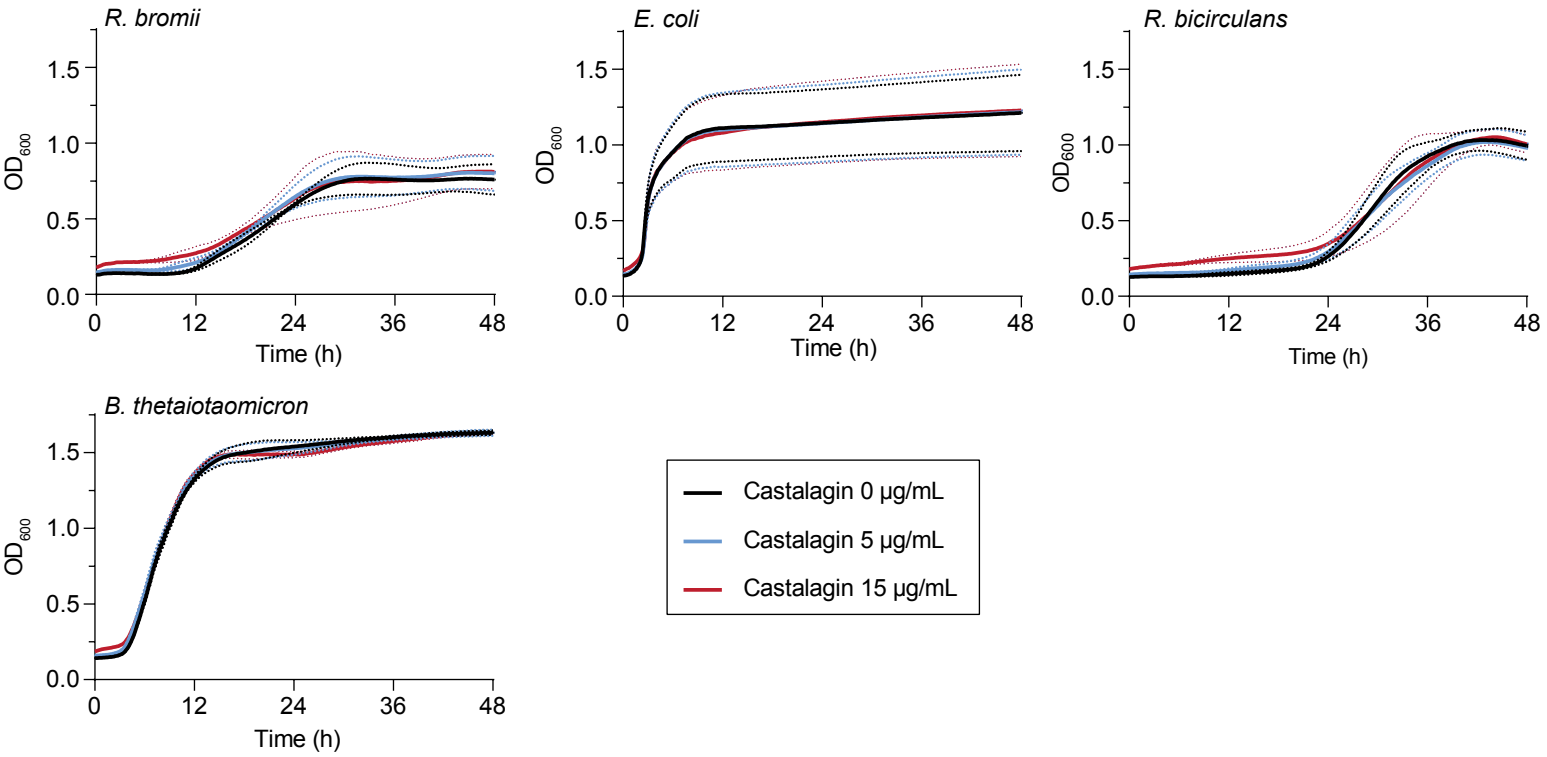

Supplementary Figure S16. Bacterial growth curves in the presence of castalagin. Growth curves of *R. bromii, Escherichia coli, R. bicirculans,* and *Bacteroides thetaiotaomicron* in ABB medium containing castalagin at a concentration of 0, 5, or 15 µg/ml. Cell growth was monitored by measuring the optical density at 600 nm. Each curve is the mean (solid line) ± SEM (dotted line) of three independent experiments.

Supplementary Figure S17

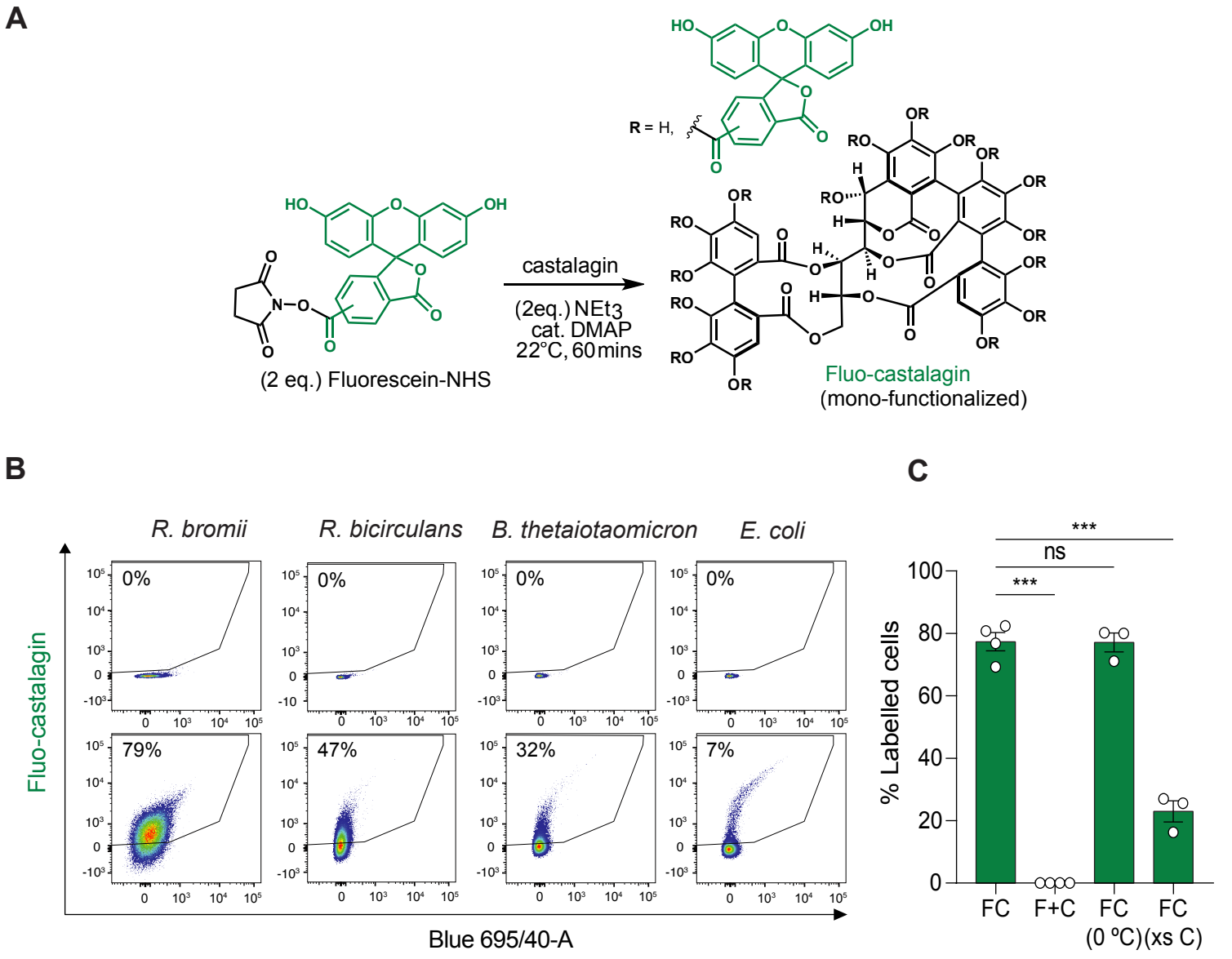

Supplementary Figure S17. Interaction of castalagin with specific bacteria. A. Fluo-castalagin probe synthesis scheme. **B.** Density plots of one representative flow cytometry labelling experiment on *R. bromii, E. coli, and B. thetaiotaomicron.* Cells in the top panels were incubated with free fluorescein and free castalagin (2 µM each), whereas cells in the bottom panels were incubated with 2 µM fluo-castalagin. **C.** Mean ± SEM of labelling experiments with *R. bromii*. Cells were incubated with either 2 µM fluo-castalagin (FC) or 2 µM free fluorescein and free castalagin (F+C) for 1 hour. Unless otherwise specified, all incubations were done at 37 °C. As a control for active uptake, *R. bromii* was incubated with FC at 0 °C. As a control for probe specificity, *R. bromii* was incubated with an excess of free castalagin (xs C) at 100X concentration of the probe immediately before the addition of FC. One-way ANOVA with Dunnett's multiple comparisons test was used to compare all groups to FC. ***$p < 0.001$.

Supplementary Figure S18

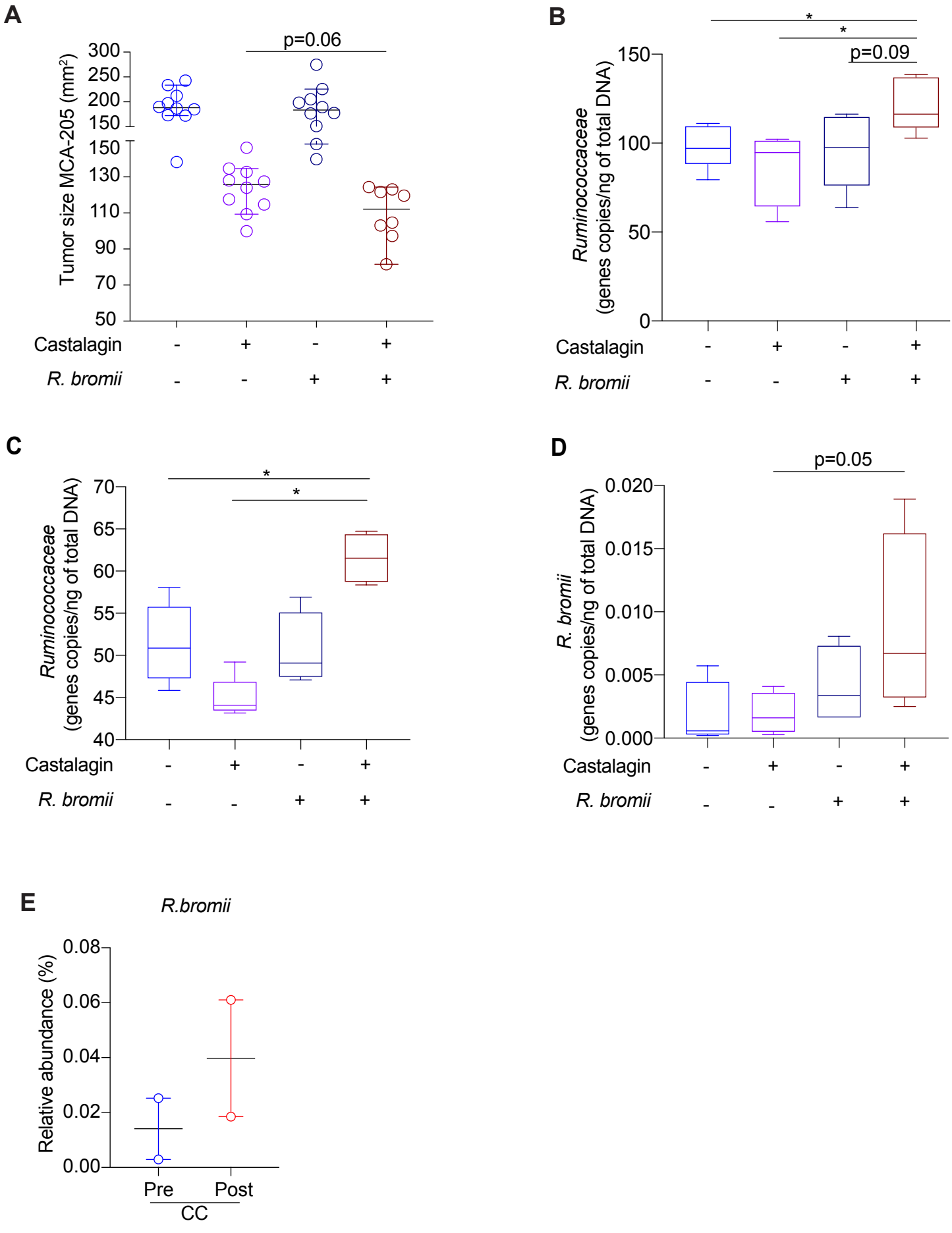

Supplementary Figure S18. In vivo experiments demonstrating relationship between castalagin and *Ruminococcus*. A. Oral administration of *R. bromii* every second days in recipient mice in MCA-205 tumor model, treated with or without castalagin. Real-time PCR of DNA extracted from mouse feces after 6 days of oral gavage with water or castalagin and with or without oral gavage of *R. bromii* using specific primers for Ruminococcaceae in the GF mice experiment **(B)** or SPF experiment **(C)** and specific primers for *R. bromii* detection **(D)** in the MCA-205 experiment (n=5/group). Means ± SEM are *$p < 0.05$. **E.** Shotgun sequencing of fecal samples taken from two non-cancer patients at pre-treatment (PRE) and paired to 4 weeks post-treatment (POST) of daily intake of 1.5 mg CC, showing relative abundance of *R. bromii*.

Supplementary Table S1. Baseline characteristics of patients with NSCLC selected for the FMT experiments

Characteristics	Non-responders (NR)						Responders (R)			
	NR1	NR2	NR3	NR4	NR5	NR6	R1	R2	R3	R4
Age	67	72	70	59	78	56	58	66	78	60
Sex	Female	Female	Female	Female	Female	Female	Female	Female	Male	Female
Smoking history	Yes	Yes	Yes	Yes	No	No	Yes	Yes	No	No
ECOG	1	0	1	1	1	1	0	0	0	2
Stage	IV	IV	IV	IV	IV	IV	IIIA*	IV	IV	IV
Histology	Adenocarcinoma	Adenocarcinoma	Adenocarcinoma	Adenocarcinoma	Adenocarcinoma	Adenocarcinoma	Adenocarcinoma	Adenocarcinoma	Adenocarcinoma	Adenocarcinoma
PD-L1 expression	>50%	>50%	>50%	>50%	1-49%	>50%	>50%	<1%	<1%	>50%
Prior chemotherapy	No	Yes	Yes	No	No	Yes	Yes	Yes	No	Yes
ICI type	Pembrolizumab	Pembrolizumab	Nivolumab	Pembrolizumab	Pembrolizumab+ Chemotherapy	Nivolumab	Pembrolizumab	Nivolumab	Pembrolizumab	Pembrolizumab
Objective response rate	PD	PD	PD	PD	PD	PD	PR	PR	PR	PR
OS (month)	0.9	13.3	5.6	10.2	9.6	4.3	17.9	21.7	17.5	12.7

ECOG; Eastern Cooperative Oncology Group. ICI; immune checkpoint inhibitors.
PD; progressive disease. PR; partial response. OS; Overall survival
*Treated as advanced cancer, not amenable to definitive treatment

Supplementary Table S2. List of bacteria increased in CC/IsoPD1 compared to Water/IsoPD1 in NR FMT.

	log2FoldChange	p value
Bifidobacteriaceae	11,60	≤0.00001
Bifidobacterium	11,28	≤0.00001
Carnobacteriaceae	2,78	≤0.00001
Staphylococcaceae	5,60	0,0003
Staphylococcus	5,02	0,005
Ruminococcaceae	0,80	0,054
Ruminococcaceae UCG-009	5,28	0,056
Peptostreptococcaceae	1,40	0,10
Oscillibacter	0,55	0,14
Lachnospiraceae UCG-006	0,82	0,16
Ruminococcaceae UCG-014	0,48	0,17
Acetatifactor	0,87	0,17
Lachnospiraceae	0,72	0,18
Christensenellaceae	1,98	0,19

Supplementary Table S3. Baseline characteristics of patients with NSCLC selected for castalagin metabolism experiments

Characteristics		Non-responders (NR) (n=12)	Responders (R) (n=11)
Age-yr	Range (median)	56-78 (68)	60-84 (70)
Sex- no (%)	Male	5 (41.7%)	5 (45.4%)
	Female	7 (58.3%)	6 (54.6%)
Smoking history-no. (%)	Yes	2 (16.7%)	5 (45.4%)
	No	10 (83.3%)	6 (55.6%)
ECOG performance status – no. (%)	0	4 (33.3%)	5 (45.4%)
	1	7 (58.4%)	4 (36.4%)
	2	1 (8.3%)	2 (18.2%)
Stage- no (%)	IIB	0 (0.0%)	1 (9.1%)
	IIIA	0 (0.0%)	1 (9.1%)
	IIIB	2 (16.7%)	1 (9.1%)
	IV	10 (83.3%)	8 (72.7%)
Histology- no (%)	Adenocarcinoma	8 (66.6%)	9 (81.8%)
	Squamous	3 (25%)	2 (18.2%)
	Others	1 (8.3%)	0 (0.0%)
PD-L1 expression- no (%)	<1%	3 (25%)	1 (9.1%)
	1-49%	4 (33.3%)	3 (27.3%)
	>50%	5 (41.7%)	7 (63.6%)
Prior chemotherapy - no (%)	Yes	2 (16.7%)	4 (36.4%)
	No	10 (83.3%)	7 (63.6%)
ICI type	Pembrolizumab	5 (41.7%)	7 (63.6%)
	Nivolumab	1 (8.3%)	2 (18.2%)
	Durvalumab	3 (25%)	0 (0.0%)
	Pembrolizumab+chemotherapy	3 (25%)	2 (18.2%)
Objective response rate-no (%)	PD	10 (83.3%)	0 (0.0%)
	SD	2 (16.7%)	5 (45.5%)
	PR	0 (0.0%)	5 (45.4%)
	CR	0 (0.0%)	1 (9.1%)
OS (month)	Range (median)	3.3-30.3 (7.7)	7.5-41.4 (15.6)

ECOG; Eastern Cooperative Oncology Group. ICI; immune checkpoint inhibitors.

PD; progressive disease. SD; stable disease. PR; partial response. CR; complete response

OS; overall survival

Supplementary Table S4. List of antibodies used for the membrane flow cytometry staining

Target	Clone	Supplier
CD3	145-2C11	Biolegend
CD4	GK1.5	Biolegend
CD8	53-6,7	Biolegend
CD44	IM7	Biolegend
CD45	30-F11	Biolegend
CD45RB	C363-16A	Biolegend
CD62L	MEL-14	Biolegend
Foxp3	FJK-16s	Biolegend
CXCR3	CXCR3-173	Biolegend
CCR9	CW-1.2	Biolegend
PD-1	29F.1A12	Biolegend
PD-L1	MIH5	BD
ICOS	7E.17G9	Biolegend

Supplementary Table S5. List of antibodies used for immunofluorescence staining.

IF antibodies Primary/Secondary	Target	Isotype	Conjugate	Clone	Supplier
Primary	Mouse CD4	Rat IgG_{2a}	AF-647	RM4-5	BD Biosciences
	Mouse CD8		AF-488	53-6.7	BD Biosciences
	Mouse FoxP3		Biotin	FJK-16s	ThermoFisher
Secondary	Goat	Donkey whole IgG	AF-488	705-546-147	Jackson ImmunoResearch
	Rat			Polyclonal	ThermoFisher

Supplementary Materials and Methods

HPLC and LC-MS systems. A 1260 Infinity LC system connected to a 6120 Quadrupole LC/MS mass spectrometer (MS) from Agilent Technologies was used for reversed-phase chromatography and mass spectrometry. A two-component solvent system of MilliQ water (solvent A) and acetonitrile (ACN, Sigma) (solvent B) was used. Each solvent was acidified with formic acid (FA, Sigma) to a final concentration of 0.1%. For LC-MS analysis, only negative ionization data are reported as this MS polarity was optimal for polyphenols in acidified solutions.

Identification of the active fraction P (fractionation round 1). To discover which compounds in CC were responsible for its antitumor activity, four fractions were produced by reversed-phase chromatography and sequential extraction: polar (P), medium polarity (MP), non-polar (NP), and insoluble (INS). Polyphenols were extracted from CC and concentrated to dryness, then re-dissolved in a mixture of 40% ACN:10% MeOH in water to solubilize most polyphenols. Insoluble material was separated by filtration and discarded. The same solvent gradient used for CC peak identification (above) was used for preparative HPLC. A Waters X-Select CSH (C18, 10 X 150 mm, 5 μm) column was used with a flow rate of 4.72 mL/min. Fractions were manually collected every 10 min for a total of 60 min. Fractions were then frozen at -80 °C and lyophilized. The three fractions from 30-60 min were combined to produce fraction NP.

The HPLC column breakthrough from 0-10 min was used as a starting point to produce fraction P. Briefly, four Strata C18-E (1 g / 6 mL) solid-phase extraction (SPE) columns (Phenomenex), were set-up in parallel and conditioned with MeOH. The lyophilized 0-10 min HPLC breakthrough was dissolved in MilliQ water to a concentration of 10 mg/mL. Five millilitres of sample (10 mg/mL) were added to each column and the flow-through was collected. Then, 9 mL of 5% ACN was added to the column and the flow-through was collected. Collected flow-throughs from each column were combined and lyophilized to produce fraction P.

Fraction MP and INS were produced through successive extractions of CC powder with water, to remove highly polar compounds, then with 50% MeOH, then 90% MeOH.

Fraction M was composed of the 50% MeOH extract, which was evaporated then lyophilized. The INS fraction was composed of the dried subsidence after all extraction steps were completed.

Identification of the active sub-fraction P3 (fractionation round 2). To discover which compounds in fraction P were responsible for antitumor activity, four sub-fractions were produced. As for the production of fraction P, the HPLC breakthrough from 0-10 min (fractionation round 1), which was dissolved in MilliQ water, was used as a starting point for fractionation round 2. A Waters X-Select HSS (C18, 10 X 150 mm, 5 µm) column was used with a flow rate of 4.72 mL/min. A new solvent gradient was developed to focus on polar polyphenols that were contained in fraction P. The gradient method was as follows: 0% B at 0 min, 16% B at 30 min, 95% B at 35 min, 100% B from 36-46 min. Fractions were manually collected every minute for 30 minutes, then recombined to produce fractions P1 (0-5 min), P2 (5-17 min), P3 (18-19) and P4 (20-30) (Supplementary Fig. S7).

Sub-fraction P3 characterization. The purity of the castalagin peak in sub-fraction P3 was determined by peak integration of the 254 nm analytical LC-MS chromatogram. A castalagin analytical standard (PhytoProof©, Sigma-Aldrich) dissolved in MilliQ water was used for comparison of both retention times (254 nm) and negative ion mass spectra. Both sub-fraction P3 and the castalagin analytical standard were dissolved in D_2O for analysis by NMR. ^{1}H, ^{1}H-^{1}H correlated spectroscopy (COSY) and ^{1}H-^{13}C heteronuclear single quantum coherence (HSQC) NMR spectra were recorded on a Bruker AVIIIHD 500 MHz NMR spectrometer. Data were visualized in TopSpin 4.0.7 (Bruker). The DHO residual solvent peak was set to 4.79 ppm for all ^{1}H NMR spectra. Peaks were assigned using the castalagin structural reassignment by Matsuo et al., 2015 (2) as a starting point.

Castalagin and vescalagin isolation from food-grade oak. Lightly toasted American oak chips (Canadian Home Brew Supplies) were extracted in a 1:13 ratio (g:mL) three times in 70% acetone in water. The extract was evaporated to remove the acetone and then lyophilized. Lyophilized extract was re-dissolved in a minimal volume of 5% ACN. Castalagin and vescalagin were subsequently purified by preparative HPLC. Both

castalagin and vescalagin from oak were dissolved in D_2O for analysis by NMR. ^1H, ^1H-^1H correlated spectroscopy (COSY) and ^1H-^{13}C heteronuclear single quantum coherence (HSQC) NMR spectra were recorded on a Bruker AVIIIHD 500 MHz NMR spectrometer. Data were visualized in TopSpin 4.0.7 (Bruker). The DHO residual solvent peak was set to 4.79 ppm for all ^1H NMR spectra. Peaks were assigned using the castalagin structural reassignment by Matsuo et al., 2015 (2) as a starting point.

Minimum medium (MM) recipe. MM was composed of the following components at final concentrations: 6.6 mM KH_2PO_4 (BioShop Canada), 15 mM NaCl (BioShop Canada), 100 µM $MgCl_2$ (BioShop Canada), 175 µM $CaCl_2$ (Fisher), 50 µM $MnSO_4$, 5 mM $(NH_4)_2SO_4$ (BioShop Canada), 15 µM $FeSO_4$ (BioShop Canada), 24 µM $NaHCO_3$ (Fisher), 6 µM hemin (Sigma), 1.9 µM hematin (Sigma), 200 ng/mL vitamin B12 (BioShop Canada), and 1 mg/mL L-cysteine (BioShop Canada). The solution was then filter-sterilized through a 0.22 µm syringe filter.

Bacterial growth curves. Stationary-phase cultures (10 µL) were diluted into 180 µL of fresh ABB medium in each well of a sterile 96-well plate (Corning). Then, 10 µL of 20X castalagin stock solutions (0, 100, 300 µg/mL in water) were added to each well. Three technical replicates were included for each condition in each experiment. The 96-well plate was incubated at 37 °C in a plate reader (Epoch 2, BioTek) and the optical density at 600 nm (OD_{600}) was monitored every 10 min for at least 48 hours. The entire experiment was performed in an anerobic chamber.

Immunofluorescence staining analysis. Different Analysis Protocol Packages (APPs) were created and applied in batch process to the images to determine cell subtypes as follows:

First, an APP 001_Detect Tissue was created to automatically detect tissues in the images. The input magnification was 10X with a 1024x1024 pixels frame and a counting frame of 85%. The classification method used was thresholding on a F(3) feature based on the addition of a first feature F(1) of a Median filter (11x11) on the FITC channel and a second feature F(2) of a Median filter (41x41) on the DAPI channel. Several post-processing steps

were applied to affine the classification: filled holes with an area smaller than 5000 μm^2 and cleared detection with an area smaller than 10000 μm^2. Manual modifications were realized to clear overlaps of tissues or debris detections not linked to cell expression. A second APP 002_Tissue Calcul was batch processed on the images to calculate the Total Area of the Tissue detected by the first APP. The third APP 003_Detect Nuclei was developed differentially depending on the batch of tumor images. All APPs 003 used an input magnification of 20X with a 1024x1024 pixels frame and a counting frame of 70 to 80%. The nuclei were classified by a thresholding method, either using a Median (9x9) filter or a Median Unsharp filter (33x33). In the post-processing steps, nuclei were separated using a PolyBlobs featured on the DAPI channel ((27x27)^3 or (43x43)^2 filter; object diameter between 6 to 10 µm, assuming that objects were elliptics) as object heatmap. Nuclei with an area inferior to 6 μm^2 were cleared. The number of nuclei was then calculated using the counting frame. Finally, a last APP 004_Panel 1 Detection was batch processed on the images to classify the different cell subtypes ($CD8^+CD4^-FoxP3^-$; $CD8^-CD4^+FoxP3^-$; $CD8^-CD4^+FoxP3^+$). In this APP, the input magnification used was 20X with a 1024x1024 pixels frame and a counting frame of 70%. All classifications were based on intensity of expression in each nuclei of the different markers after filtering each signal as follow: for CD8 channel, the background was normalized using the substract background filter (50% with Dark background), then a Median filter (5x5) was used; for CD4 channel, a Median Unsharp filter (11x11) followed by a Median filter (7x7) was used; and for the FoxP3 channel, a Median filter (7x7) was used. Each threshold was adapted through the different images before batch processing. The proportion of each cell subtype was finally calculated using the counting frame (count and area).

***In vivo* killing assay.** *in vivo* killing assay was performed through the intravenous (i.v.) injection of CFSE-labeled target cells as described by Oster P. *et al* (3). Recipient naive 8-12 week-old C57BL/6 female mice were treated by oral gavage with Castalagin (n=10) or water (n=10) for 8 days. On day 3, they were injected i.v. with $1x10^6$ $CD45.1^+$ OT-1 $CD8^+$ T lymphocytes, isolated from the lymph nodes and spleen of OT-1 mice using the $CD8a^+$ T Cell Isolation kit (MACS, Miltenyi Biotech GMBH, Solothurn, Switzerland). On day 4, the recipient mice were immunized once with 10 µg Ova peptide (SIINFEKL) and

50 μg CpG in 100 μL PBS through subcutaneous injection on the flank. On day 7, the recipient mice were infused with splenocytes extracted from naive 8-12 week-old female C57BL/6 donor mice. Prior injection, the splenocytes were loaded with OVA peptide (200μM) or left unloaded. Pulsed cell were labeled with 0.5μM CFSE (CFSE, Enzo life Sciences, Lausen, Switzerland), resulting in a $CFSE^{low}$, population and unpulsed cell were labeled with 5 μM CSFE, resulting in a $CFSE^{high}$ population. A mixture of the two labelled cell populations (1:1 ratio) was i.v injected into recipient mice. Fourteen hours post injection, the spleens of recipient mice were recovered and the ratio between the $CFSE^{low}$ and $CFSE^{high}$ fraction was determined by flow cytometry to assess killing activity of OT-1 cells.

Quantitative real-time PCR (qRT-PCR). qRT-PCR was performed to evaluate the relative levels of the total bacterial DNA, and the V6 region of the 16S rRNA gene was amplified using the primer set 891F (5'-TGGAGCATGTGGTTTAATTCGA-3' and 1033R (5'-TGCGGGACTTAACCCAACA-3') (4). The relative levels of the Ruminococcaceae DNA was determined using the specific primers F (5'-ACTGAGAGGTTGAACGGCCA-3') and R (5'-CCTTTACACCCAGTAAWTCCGGA-3') (5). The relative levels of the *R. bromii* DNA was determined using the specific primers RBR-5 (5′- GAA GTA GAG ATA CAT TAG GTG -3′) and RBR-6 (5′- ACG AGG TTG GAC TAC TGA -3′) (6). Extracted DNA (400 ng/well) was combined with 500 nM of the above described primer mix and 1X qPCRBIO SyGreen Blue Mix Hi-ROX (PCRBIOSystems). Raw threshold cycle (Ct) values were compared to a bacterial standard curve produced with Escherichia coli DNA for the 16S analysis and with *R. bromii* for the Rumniccocaceae and *R. bromii* analysis for approximation of bacterial load in ng was determined in the 400ng total bacterial DNA.

16S rRNA gene sequence processing and analysis of mouse feces samples. The V3–V4 region of the 16S rRNA gene was amplified by PCR using primers Bakt_341F (5′-CCTACGGGNGGCWGCAG-3′) and Bakt_805R (5′-GACTACHVGGGTATCTAATCC-3′), which were adapted to incorporate the transposon-based Illumina Nextera adapters (Illumina) and a sample barcode sequence allowing

multiplexed paired-end sequencing. PCR mixtures contained 1× Q5 buffer (NEB), 1× Q5 Enhancer (NEB), 200 μM dNTP (VWR International), 0.2 μM of forward and reverse primers (Integrated DNA Technologies), 1 unit of Q5 (NEB) and 1 μl of template DNA in a 50 μl reaction. The PCR cycling conditions consisted of an initial denaturation of 30 sec at 98°C, followed by a first set of 15 cycles (98°C for 10 sec, 55°C for 30 sec and 72°C for 30 sec), then by a second step of 15 cycles (98°C for 10 sec, 65°C for 30 sec and 72°C for 30 sec) and a final elongation of 2 min at 72°C before cooling to 4°C indefinitely. PCR products were purified using 35 μL of magnetic beads (AxyPrep Mag PCR Clean up kit; Axygen Biosciences) per 50 μL PCR reaction. Amplifications were controlled on a Bioanalyzer 2100 using DNA 7500 chips (Agilent Technologies). Samples were pooled at an equimolar ratio; the pool was repurified as described before (4) and checked for quality on a Bioanalyzer 2100 using a DNA high sensitivity chip. The pool was quantified using picogreen (Life Technologies) and loaded on a MiSeq system (Illumina). High-throughput sequencing was performed at the IBIS (Institut de Biologie Intégrative et des Systèmes - Université Laval).

Gene sequence processing and analysis was performed using R v4.0.0. DADA2R package v1.16.0 (7) was used to generate exact amplicon sequence variants (ASV) of each sample from raw amplicon sequences. Sequences were corrected for Illumina amplicon sequence errors, de-replicated, chimera removed, and merged for paired-end reads, with 260-bases for forward reads and 190-bases for reverse reads. The taxonomy assignment was performed against the SILVA reference database v138 (8). Archaea and Eukaryota residual sequences were removed. Downstream analyses were performed at the genus level through phyloseq R package v1.32.0 (9).

RNA sequencing and analysis. RNA was extracted from mouse tumors using the Maxwell RSC simplyRNA Tissue kit (Promega) according to the manufacturer's protocol. RNA quality was assessed by spectrophotometry with absorbance at 230, 260, and 280 nm. DNA was quantified using the Qubit fluorometric assay (Life Technologies). The rRNA-depleted RNA was used for the library preparation with the NEBNext Ultra II Directional RNA library prep kit for Illumina (New England Biolabs) according to the manufacturer's instructions. Libraries were paired-end sequenced (2x76 base pairs) on a NextSeq500

device (Illumina), with a read depth of 20 million. Kallisto software (10) was used for quantifying transcript abundance from RNA-seq data against the GRCm39 cDNA reference transcriptome from the Ensembl database, release 103. Only protein-coding transcripts and genes were included in the downstream analysis. Differential expression analysis was performed using the DESeq2 R package (11). Gene Set Enrichment Analysis (GSEA) was performed using the clusterProfiler R package (12). The CIBERSORT tool was used to estimate the abundances of tumor-infiltrating immune cells (13).

Metagenomics sequencing and analysis.

Library construction and sequencing. gDNA was quantified using the Quant-iT™ PicoGreen® dsDNA Assay Kit (Life Technologies). Libraries were generated from 50ng of gDNA using the NEBNext Ultra II DNA Library Prep Kit for Illumina (New England BioLabs) as per the manufacturer's recommendations. Adapters and PCR primers were purchased from IDT. Size selection of libraries contained the desired insert size has been performed using SparQ beads (Qiagen). Libraries were quantified using the Kapa Illumina GA with Revised Primers-SYBR Fast Universal kit (Kapa Biosystems). Average size fragment was determined using a LabChip GXII (PerkinElmer) instrument.

The libraries were normalized and pooled and then denatured in 0.05 N NaOH and neutralized using HT1 buffer. The pool was loaded at 225 pM on an Illumina NovaSeq S4 lane using Xp protocol as per the manufacturer's recommendations. The run was performed for 2x150 cycles (paired-end mode). A phiX library was used as a control and mixed with libraries at 1% level. Base calling was performed with RTA v3.4.4 . Program bcl2fastq2 v2.20 was then used to demultiplex samples and generate fastq reads.

Sequencing data preprocessing. First, quality control was performed with fastp (14): 1) Illumina sequencing adapters were removed 2) low quality reads were trimmed and 3) read too short (< 60 bp) were discarded. Then, reads mapped to the mouse genome (GCF_000001635.27) with bowtie2 (15) were removed. Finally, 35M high-quality read pairs were randomly selected in each sample with fastq-sample (https://github.com/fplaza/fastq-sample).

Gene abundance table generation. The gene abundance table was generated with the METEOR software suite (https://forgemia.inra.fr/metagenopolis/meteor) . First, 70M

selected high quality reads were mapped with bowtie2 to the 5.0 mimic2 gene catalog of the mouse gut microbiota https://doi.org/10.15454/L11MXM constructed in the framework of the study using assemblies obtained from the 68 samples of the present study. Alignments with nucleotide identity < 95% were discarded and gene counts were computed with a two-step procedure previously described (16) that handles multi-mapped reads. The samples mapped with high and homogenous mapping percentage to the catalogue (mean 78 ± 2%). Finally, raw gene counts were normalized according to gene length.

MetaGenomic Species abundance table generation. The abundance of a MetaGenomic Species (MGS) in a sample was defined as the mean abundance of its 100 marker genes (i.e. species-specific core genes that correlate the most altogether). If less than 10% of the marker genes were seen in a sample, the abundance of the MGS was considered as null.

Ex vivo castalagin metabolism assay. Twenty three frozen human stool samples from different non-small cell lung cancer (NSCLC) patients amenable to immune checkpoint inhibitors (ICIs) after patient records were retrospectively analyzed to identify their response status and their baseline clinical characteristics (Supplementary Table S2). The stool samples were suspended in modified ABB medium (without iron sources, mABB) at a 1:10 (g:mL) ratio and homogenized using a serological pipette (0.1 g stool/condition tested). The resulting slurries were centrifuged at 700 x g for 3 min and the supernatant (containing bacteria) was transferred to a new tube. The supernatant was centrifuged at 6,500 x g for 5 min to pellet bacteria. The pellet was then washed with mABB and centrifuged once more at 6,500 x g for 5 min. Stool bacteria were resuspended in mABB to a final volume of 300 µL/0.1 g stool mass. Three conditions were routinely employed for each sample: vehicle (control for bacterial matrix), castalagin (99 µM), and heat-shocked slurry (80 °C for 10 min) + castalagin (99 µM) (control for non-enzymatic degradation). Three hundred µL of fecal slurry were used for each condition. Media only and media + castalagin (99 µM) controls were included to control for media components and abiotic degradation of castalagin, respectively. All samples and controls were incubated at 37 °C for 48 h, then frozen at -80 °C or extracted immediately.

Samples and controls (300 µL) were spiked with salicylic acid (internal standard (IS), 362 µM) and vortexed. Three times the media volume (900 µL) of ethyl acetate + 1% formic

acid were added to each tube and the contents were vortexed. Layers were separated by centrifuging at 10,000 x g for 5 min and the organic layer was transferred to a new tube. The organic layer was dried using a speedvac concentrator (Heto Lab) set to 40 °C to accelerate solvent evaporation. Dried extracts were resuspended in 150 µL of 30% ACN, vortexed, and centrifuged at 20,000 x g for 5 min to pellet insoluble materials.

Urolithins were analyzed by LC-MS by injecting 10 µL of sample into an Agilent Poroshell 120 EC-C18 column (4.6 x 50 mm, 2.7 µm) fitted with a guard column (4.6 x 5 mm, 2.7 µm). A solvent flow rate of 0.7 mL/min was used throughout the method and the gradient was as follows: 10% B at 0 min, 30 % B at 8 min, 100% B from 10-13.5 min.

Retention times and mass spectra for peaks of interest were compared to authentic standards when available (urolithin D, urolithin C, isourolithin A, urolithin A, urolithin B (Toronto Research Chemicals), and ellagic acid (Sigma)). Analyte peak areas (305 nm) were integrated and normalized to the internal standard area for each sample or control (analyte/IS). Patient urolithin metabolic phenotypes (metabotypes) were stratified according to the final urolithins produced in ex vivo metabolism assays: metabotype A (urolithin A exclusively), metabotype B (isourolithin A and/or urolithin B), and metabotype 0 (none of the final metabolites) (1).

Modified Anaerobe Basal Broth recipe (mABB). A modified ABB medium was made due to global supply shortages and to minimize precipitation of castalagin when used at high concentrations. The following components were mixed together and autoclaved: 16 g/L peptone (BioShop Canada), 7 g/L yeast extract (BioShop Canada), 5 g/L NaCl (BioShop Canada), 1 g/L starch (from potato) (Sigma), 1 g/L D-glucose (BioShop Canada), 1 g/L sodium pyruvate (BioShop Canada), 0.5 g/L sodium succinate (Sigma), 0.5 g/L sodium thioglycolate (TCI), and 15 g/L agar (when making plates) (Fisher). Media was cooled after autoclaving and the following filter-sterilized components (stock solutions) were added aseptically to the following final concentrations: 1 g/L L-arginine (BioShop Canada), 0.5 g/L L-cysteine HCl (BioShop Canada), 0.4 g/L sodium bicarbonate (BioShop Canada), vitamin K1 0.5 mg/L (dissolved in 95% EtOH, Sigma), 1 g/L dithiothreitol (DTT, Fisher).

Metabolomics experiment and analysis.

Tissue and serum sample preparation. Collected tissues fecal contents and feces were weighted (30 mg) in a 2 mL-homogenizer tube with ceramic beads (Hard Tissue Homogenizing CK28, 2.8 mm zirconium oxide beads; Precellys, Bertin Technologies, France). Next, 1 mL of ice-cold extraction mixture (MeOH/water, 9/1, -20°C, with a cocktail of internal standards), was added to the homogenizer tube. Samples were completely homogenized (3 cycles of 20 s at 5000 rpm; Precellys 24, Bertin Technologies, Montigny-le-Bretonneux, France), to facilitate solvent access and endogenous metabolites extraction. Homogenates were then centrifuged (10 min at 15000 g, 4°C), and supernatants were collected.

Serum samples (25 µL) were mixed with 250 µL of the of ice-cold extraction mixture, allowing protein precipitation and metabolites extraction, then vortexed and centrifuged (10 min at 15000 g, 4°C). After sample (tissues/feces or Serum) centrifugation, supernatants were collected, split in 3 fractions, and treated according to the protocols described in Grajeda-Iglesias C. et al. (17). Briefly, 3 fractions of sample extract were split. The 1st fraction for short chain fatty acids analysis, the 2nd fraction for LC/MS and the 3rd fraction for GC/MS analyses. Finally, a 4th fraction was re-extracted from the pellet for polyamines analysis.

UHPLC/MS. Targeted UHPLC/MS analyses were performed on a UHPLC 1290 system (Agilent Technologies, Waldbronn, Germany), with an autosampler kept at 4°C, and a pelletier oven for rigorous control of the column temperature. The UHPLC was coupled to a QQQ/MS 6470 (Agilent Technologies) equipped with an electrospray source, using nitrogen as a collision gas. For detection of short chain fatty acids and ketone bodies in the 1st fraction, 10 µL of sample were injected into a Zorbax Eclipse XDB-C18 (100 mm x 2.1 mm, particle size 1.8 µm; Agilent) column protected by a guard column C18 (5 mm × 2.1 mm, particle size 1.8 µm). The column oven was maintained at 50°C during analysis. The gradient mobile phase consisted of 0.01 % formic acid (Sigma-Aldrich) (A) and ACN (0.01 % formic acid) (B). The flow rate was set to 0.7 ml/min, and gradient as follow: 20% B (initial conditions) maintained for 3 min, to 45% B in 4 min; then 95% B maintained 2 min, and finally equilibration to initial conditions, 20% B, for 1 min. The QQQ/MS was operated

in negative mode. The gas temperature was set to 300°C with a gas flow of 12 L/min. The capillary voltage was set to 5 kV.

For detection of bile acids, 5 µL from samples recovered in water (2nd fraction), were injected into a Poroshell 120 EC-C8 (100 mm x 2.1 mm particle size 2.7 µm; Agilent technologies) column protected by a guard column (XDB-C18, 5 mm × 2.1 mm particle size 1.8 µm). Mobile phase consisted of 0.2% formic acid (A) and ACN/IPA (1/1; v/v) (B) freshly made. Flow rate was set to 0.5 mL/min, and gradient as follow: 30% B increased to 38% B over 2 min; maintained for 2 minutes then increased 60% for 1.5 minutes, and finally to 98% B for 2 minutes (column washing), followed by 2 min of column equilibration at 30% B (initial conditions). The QQQ/MS was operated in negative mode. Gas temperature and flow were set to 310°C and 12 L/min, respectively. Capillary voltage was set to 5 kV.

Polyamines were detected in the 4th fraction after injection of 10 µL of sample into a Kinetex C18 (150 mm x 2.1 mm particle size 2.6 µm; Phenomenex) column protected by a guard column C18 (5 mm × 2.1 mm, particle size 1.8 µm). Column oven was maintained at 40°C during analysis. The gradient mobile phase consisted of 0.1 % HFBA (Sigma-Aldrich) (A) and ACN (0.1 % HFBA) (B) freshly made. The flow rate was set to 0.4 ml/min, and gradient as follow: from 5% (initial conditions) to 30% B in 7 min; then 90% B maintained 2 min, and finally equilibration to initial conditions, 5% B, for 2 min. The QQQ/MS was operated in positive mode. The gas temperature was set to 350°C with a gas flow of 12 L/min. The capillary voltage was set to 2.5 kV.

In addition, tissue samples were injected for the analysis of nucleotides and co-factors into a Zorbax Eclipse plus C18 (100 mm × 2.1 mm, particle size 1.8 µm, Agilent) column protected by a guard column C18 (5 mm × 2.1 mm, particle size 1.8 µm). Column oven maintained at 40°C during analysis. The gradient mobile phase consisted of 0.5 mM DBAA (Sigma-Aldrich) (A) and ACN (B). The flow rate was set to 0.4 ml/min, and gradient as follow: 10% B (initial conditions) maintained for 3 minutes, then increased to 95% B in 1 min and maintained 2 min, to finally equilibrate to initial conditions, 10% B, for 1 min. The QQQ/MS was operated in both positive and negative mode. The gas temperature was set to 350°C with a gas flow of 12 L/min. The capillary voltage was set to 4.5 kV in positive mode and 5 kV in negative mode.

Peak detection and integration were performed using the Agilent Mass Hunter quantitative software (B.10.1).

Widely-targeted analysis of intracellular metabolites GC/MS. Derivatized samples for analysis (3rd fraction) were injected (1 µL) into a gas chromatography system (Agilent 7890B; Agilent Technologies, Waldbronn, Germany) coupled to a triple quadrupole mass spectrometer (QQQ/MS; 7000C Agilent Technologies, Waldbronn, Germany), equipped with a high sensitivity electronic impact source (EI) operating in positive mode. Injection was performed in splitless mode. Front inlet temperature was kept at 250°C, transfer line and ion-source temperature were 250°C and 230°C, respectively. Septum purge flow was fixed at 3 mL/min, purge flow to split vent operated at 80 mL/min during 1 min and gas saver mode was set to 15 mL/min after 5 min. Helium gas flowed through column (HP-5MS, 30m x 0.25 mm, i.d. 0.25 mm, d.f. J&W Scientific, Agilent Technologies Inc.) at 1 mL/min. Column temperature was held at 60°C for 1 min, raised to 210°C (10°C/min), then to 230°C (5°C/ min), to finally reach 325°C (15°C/min), and hold at during 5 min. Collision gas was nitrogen. Peak detection and integration were performed using the Agilent Mass Hunter quantitative software (B.10.1). MRM scan mode was used for targeted analysis in both GC/MS and UHPLC/MS analyses.

Pseudo-targeted analysis of intracellular metabolites. The profiling analysis was performed with a Dionex Ultimate 3000 UHPLC system (Thermo Scientific) coupled to an Orbitrap mass spectrometer (q-Exactive, Thermo Fisher Scientific) equipped with an electrospray source operating in both positive and negative mode, and acquired samples in full scan analysis mode, from 100 to 1200 m/z. LC separation was performed on a reversed phase column (Zorbax Sb-Aq 100 x 2.1 mm x 1.8 µm particle size, Agilent), with mobile phases: 0.2% acetic acid (A), and ACN (B). Column oven was kept at 40°C. Ten microliters of aqueous sample (2nd fraction) were injected for metabolite separation with a gradient starting from 2% B, increased to 95% B in 22 min, and maintained during 2 min for column rinsing, followed by column equilibration at 2% B for 4 min. Flow rate was set to 0.3 mL/min. The q-Exactive parameters were: sheath gas flow rate 55 au, auxiliary gas flow rate 15 au, spray voltage 3.3 kV, capillary temperature 300°C, S-Lens RF level 55 V. The

mass spectrometer was calibrated with sodium acetate solution dedicated to low mass calibration. Data were treated by the quantitative node of Thermo XcaliburTM (version 2.2) in a pseudo-targeted approach with a home-based metabolites list.

All targeted treated data were merged and cleaned with a dedicated R (version 4.0.1) package (@Github/Kroemerlab/GRMeta).

Supplementary references and notes.

1. Tomás-Barberán FA, García-Villalba R, González-Sarrías A, Selma MV, Espín JC. Ellagic acid metabolism by human gut microbiota: consistent observation of three urolithin phenotypes in intervention trials, independent of food source, age, and health status. J Agric Food Chem. **2014** Jul 16;62(28):6535–8.

2. Matsuo Y, Wakamatsu H, Omar M, Tanaka T. Reinvestigation of the stereochemistry of the C-glycosidic ellagitannins, vescalagin and castalagin. Org Lett. **2015** Jan 2;17(1):46–9.

3. Oster P, Vaillant L, Riva E, McMillan B, Begka C, Truntzer C, *et al*. Helicobacter pylori infection has a detrimental impact on the efficacy of cancer immunotherapies. Gut. **2021** Jul 12;gutjnl-2020-323392.

4. Anhê FF, Nachbar RT, Varin TV, Trottier J, Dudonné S, Le Barz M, *et al.* Treatment with camu camu (Myrciaria dubia) prevents obesity by altering the gut microbiota and increasing energy expenditure in diet-induced obese mice. Gut. **2019** Mar;68(3):453–64.

5. Garcia-Mazcorro JF, Suchodolski JS, Jones KR, Clark-Price SC, Dowd SE, Minamoto Y, *et al*. Effect of the proton pump inhibitor omeprazole on the gastrointestinal bacterial microbiota of healthy dogs. FEMS Microbiol Ecol. **2012** Jun;80(3):624–36.

6. Biasucci G, Benenati B, Morelli L, Bessi E, Boehm G. Cesarean delivery may affect the early biodiversity of intestinal bacteria. J Nutr. **2008** Sep;138(9):1796S-1800S.

7. Callahan BJ, McMurdie PJ, Rosen MJ, Han AW, Johnson AJA, Holmes SP. DADA2: High-resolution sample inference from Illumina amplicon data. Nat Methods. **2016** Jul;13(7):581–3.

8. Quast C, Pruesse E, Yilmaz P, Gerken J, Schweer T, Yarza P, *et al*. The SILVA ribosomal RNA gene database project: improved data processing and web-based tools. Nucleic Acids Res. **2013** Jan;41(Database issue):D590-596.

9. McMurdie PJ, Holmes S. phyloseq: an R package for reproducible interactive analysis and graphics of microbiome census data. PloS One. **2013**;8(4):e61217.

10. Bray NL, Pimentel H, Melsted P, Pachter L. Near-optimal probabilistic RNA-seq quantification. Nat Biotechnol. **2016** May;34(5):525–7.

11. Love MI, Huber W, Anders S. Moderated estimation of fold change and dispersion for RNA-seq data with DESeq2. Genome Biol. **2014**;15(12):550.

12. Wu T, Hu E, Xu S, Chen M, Guo P, Dai Z, *et al*. clusterProfiler 4.0: A universal enrichment tool for interpreting omics data. Innov N Y N. **2021** Aug 28;2(3):100141.

13. Chen B, Khodadoust MS, Liu CL, Newman AM, Alizadeh AA. Profiling Tumor Infiltrating Immune Cells with CIBERSORT. Methods Mol Biol Clifton NJ. **2018**;1711:243–59.

14. Chen S, Zhou Y, Chen Y, Gu J. fastp: an ultra-fast all-in-one FASTQ preprocessor. Bioinforma Oxf Engl. **2018** Sep 1;34(17):i884–90.

15. Langmead B, Salzberg SL. Fast gapped-read alignment with Bowtie 2. Nat Methods. **2012** Mar 4;9(4):357–9.

16. Routy B, Le Chatelier E, Derosa L, Duong CPM, Alou MT, Daillère R, *et al*. Gut microbiome influences efficacy of PD-1-based immunotherapy against epithelial tumors. Science. **2018** Jan 5;359(6371):91–7.

17. Grajeda-Iglesias C, Durand S, Daillère R, Iribarren K, Lemaitre F, Derosa L, *et al*. Oral administration of Akkermansia muciniphila elevates systemic antiaging and anticancer metabolites. Aging. **2021** Mar 2;13(5):6375–405.